SSCL-Preprint-561 Rev. 1

SSCL-Preprint-561 Rev. 1
July 1994
Distribution Category: 414

T. Sen
J. Ellison
S. Kauffmann

Collective Behavior of an Ensemble of Forced Duffing Oscillators Near the 1:1 Resonance

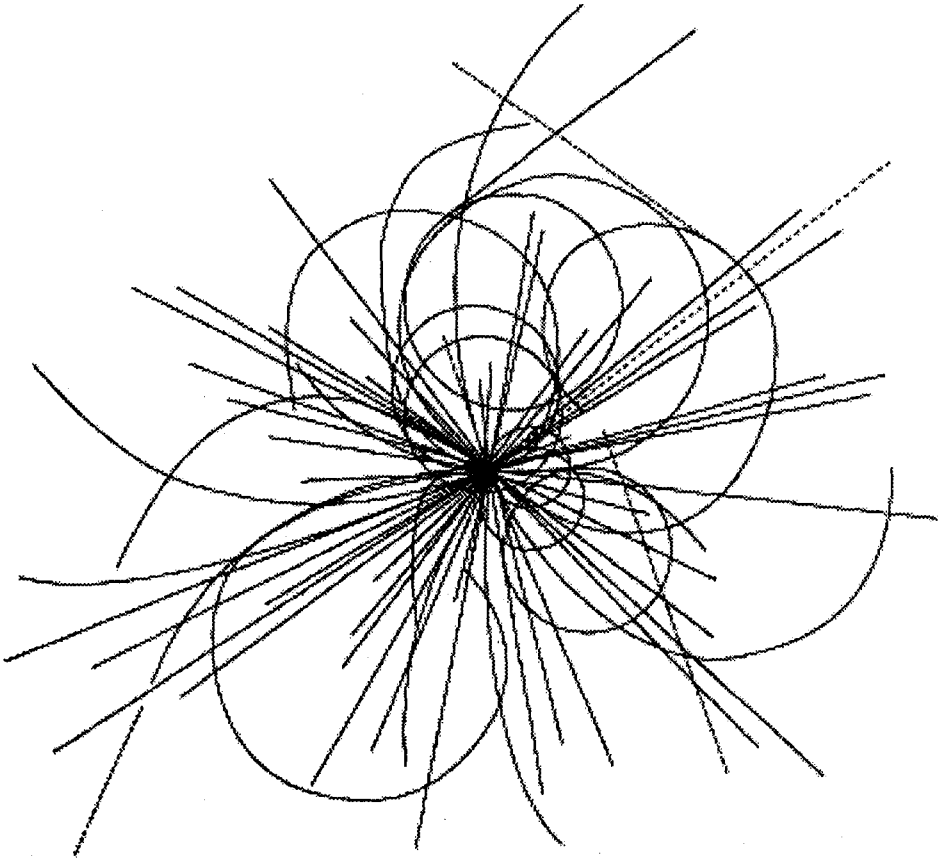

Superconducting Super Collider Laboratory

SSCL-Preprint-561 Rev. 1

Collective Behavior of an Ensemble of Forced Duffing Oscillators Near the 1:1 Resonance*

T. Sen,† J. Ellison,‡ and S. Kauffmann

Superconducting Super Collider Laboratory§
2550 Beckleymeade Avenue
Dallas, TX 75237

July 1994

* Submitted to *Physica D.*
† Address after April 15, 1994: DESY F35H, 85 Notkestrasse, 22603 Hamburg, Germany.
‡ Permanent address: Dept. of Mathematics, University of New Mexico, NM 87131.
§ Operated by the Universities Research Association, Inc., for the U.S. Department of Energy, under Contract No. DE-AC35-89ER40486.

Collective Behavior of an Ensemble of Forced Duffing Oscillators Near the 1:1 Resonance

T. Sen*, J.A. Ellison† & S.K. Kauffmann

Superconducting Super Collider Laboratory ‡
2550 Beckleymeade Avenue, Dallas, TX 75237

Preserving the beam size (or equivalently the emittance) is a primary aim of accelerator physics. Here we study the effect on the emittance of power supply ripple in the guiding magnetic fields. The collective behavior of forced Duffing oscillators is the natural model to understand this phenomenon. We consider the case when the external frequency is near the linearized natural frequency and nonlinearity and forcing are small. The method of averaging reduces the problem to an autonomous system. A coarse grained long time limit of the phase space density and the rate of approach to this limit are discussed in terms of the autonomous system. We find the frequencies which lead to the largest emittance growth in three different forcing regimes (weak, moderate and relatively large) and also characterize the dependence of emittance growth on forcing amplitude in these regimes.

Contents

1 Introduction **3**

1.1 Motivation for the Duffing equation 4

2 Collective behavior of driven linear oscillators **6**

3 Numerical solution of the Duffing equation **9**

3.1 Single particle behavior 9

3.2 Time evolution of the averaged amplitude 12

4 The averaging approximation **15**

4.1 The averaging theorem 15

---

*Address after April 15, 1994 : DESY F35H, 85 Notkestrasse, 22603 Hamburg, Germany
†Permanent address : Dept. of Mathematics, University of New Mexico, NM 87131
‡Operated by the Universities Research Association Inc., for the U.S. Department of Energy, under contract DE-AC35-89ER40486.

4.2 Fixed points of the averaged equations and their stability 17
4.3 Phase plane portraits 19
1 $\Delta < \Delta_{bf}$ 21
2 $\Delta > \Delta bf$ 23
4.4 Solution of the averaged equations 25
4.5 Fundamental frequency and Fourier coefficients of the solution 28

5 Collective behavior and the long time limit 33

6 Equilibrium density distribution 35

7 Calculation of the equilibrium density 38

8 Ensemble averages and the approach to equilibrium 42

9 Effect of detuning and forcing on amplitude growth 47
9.1 Effect of the detuning 48
9.2 Effect of the forcing amplitude 52

10 Summary 55

1. Introduction

What happens at long times to a collection of non-linear oscillators subjected to a time periodic external force? This is a question of interest both in classical and quantum physics in areas ranging from accelerator physics, plasma physics, microwave ionization of atoms, etc. The complexity of the answer depends on the number of degrees of freedom, the degree of nonlinearity and the interactions between the oscillators. One of the simplest such systems is an ensemble of one-dimensional non-interacting driven Duffing oscillators. This problem has direct application to the stability of particles in large high-energy proton accelerators in which the periodic driving comes from the ripple in the magnetic fields guiding the protons and where the Coulomb interactions amongst the protons can be neglected. The equivalence of this problem to the Duffing oscillator is derived in the following subsection 1.1.

Lately several theoretical ([1], [2], [3]) and experimental studies ([4], [5], [6]) have been performed to analyze the behavior of single particles in nonlinear fields typically present in modern accelerators. These have been driven by the desire to understand either the cause of slow particle losses due to nonlinearity or the effects of coupling between the transverse and longitudinal degrees of freedom on the longitudinal motion. Our aim here is to understand the time evolution of the transverse emittance (or beam size) due to dipole ripple resonant with the transverse motion. While the single particle dynamics of the weakly nonlinear driven Duffing oscillator is well known (see e.g. [7]) we emphasize that our interest is in the behavior of an ensemble of such oscillators.

To set the stage for our analysis, we first consider the evolution of an ensemble of driven linear oscillators in Section 2. The phase space density for this system is a quasi-periodic function of time and does not approach an equilibrium value. For driven nonlinear oscillators the behavior is quite different due to the effects of phase mixing. In Section 3 we present numerical results for the evolution of the average amplitude squared of an ensemble of Duffing oscillators. The rest of the paper is devoted to an analysis of the observed behavior. In Section 4 we discuss the averaging approximation to the Duffing equation and construct the phase space portraits and the exact solution for the averaged equations. The long time behavior of the Duffing oscillators will be understood in terms of these averaged equations. Since these equations are autonomous, the associated phase space density has a long time coarse-grained limit, the supporting arguments are given in Section 5. The construction of this equilibrium density is the subject of Sections 6 and 7. In Section 8 we discuss the ensemble averages of two quantities which characterize the particle distribution and their rate of approach to equilibrium. In Section 9 we apply our analysis to determine which drive frequencies cause the largest growth in the ensemble size and the dependence of the ensemble size at long times on the amplitude of the forcing. We sum up in Section 10. There are three appendixes, the first discusses the first order averaging theorem, the second derives the formula for the evolution

of a phase space density and the third discusses a qualitative feature of the equilibrium density. A similar problem was considered in [8] but without consideration of the approach to equilibrium and the corresponding equilibrium density, nor was the specific dependence of the emittance growth on forcing amplitude and frequency studied.

A reader interested only in the application to the accelerator problem may read the following subsection 1.1 and then proceed to Section 9 for an analysis of the effects of the ripple field on the beam emittance.

1.1. Motivation for the Duffing equation

This problem arose in the study of the effects of magnetic field ripple in electrical power supplies feeding the dipole magnets in the Collider ring at the Superconducting Supercollider. In the absence of the ripple and any magnetic field nonlinearities, the transverse motion of the circulating protons is described by the following equation [9]

$$\frac{d^2x}{ds^2} + K(s)x = 0 \ , \tag{1.1}$$

where x is the distance from the design orbit and $K(s)$ describes the strength of the quadrupole magnets as a function of the position s around the ring. Since $K(s)$ is periodic around the ring, (1.1) is a Hill's equation with two linearly independent solutions $\sqrt{\beta(s)}e^{\pm i\psi(s)}$ where

$$\psi(s) = \int_0^s \frac{ds}{\beta} \tag{1.2}$$

and β is the unique periodic solution of $2\beta\beta'' - (\beta')^2 + 4\beta^2 K(s) = 4$ with period C. Since β is periodic, $\hat{\psi}$ defined by $\psi(s) = \hat{\psi}(s) + \psi(C)s/C$ is periodic and the solutions of Hill's equations are quasi-periodic with frequencies $2\pi/C$ and $2\pi\omega_0/C$ where $\omega_0 = \psi(C)/(2\pi)$ is a dimensionless number, the so-called tune of the machine. If we make the change of dependent and independent variables by $(x, dx/ds, s) \rightarrow (\xi, \eta, \phi)$ via

$$\xi = \frac{x}{\sqrt{\beta}} \ , \quad \eta = \frac{1}{\sqrt{\beta}}\left[\beta\frac{dx}{ds} - \frac{1}{2}\frac{d\beta}{ds}x\right] \ , \quad \phi = \frac{1}{\omega_0}\psi \ ,$$

then we obtain the simple harmonic oscillator equation

$$\frac{d}{d\phi}\xi = \omega_0\eta \quad , \quad \frac{d}{d\phi}\eta = -\omega_0\xi \ ,$$

or

$$\frac{d^2\xi}{d\phi^2} + \omega_0^2\xi = 0 \ . \tag{1.3}$$

The independent variable ϕ is the betatron phase of the particle. Equation (1.3) has a conservation law

$$r_0^2 = \xi^2 + \eta^2 = \text{constant} \quad . \tag{1.4}$$

This quantity (called the Courant-Snyder invariant) times π is the area in phase space enclosed by the trajectory. For a collection of particles, it follows that the ensemble average of this quantity is preserved in the evolution. This ensemble averaged quantity

$$\epsilon = \langle \xi^2 + \eta^2 \rangle$$

is related to the "beam emittance" in usual accelerator parlance.

The presence of magnetic nonlinearities destroys the constancy of the emittance and among other things makes the tune depend quadratically on the amplitude. This can be incorporated into the equations of motion by adding a cubic non-linearity, giving

$$\frac{d^2\xi}{d\phi^2} + \omega_0^2\xi + \epsilon\alpha\xi^3 = 0 \tag{1.5}$$

where $\epsilon\alpha$ is a constant depending on the strengths of the magnetic multipoles. If there are only sextupoles and octupoles, $\epsilon\alpha$ depends on the octupole strengths to first order and the sextupole strengths to second order. Standard perturbation theory then shows that the new tune is

$$\omega = \omega_0 + \epsilon\frac{3\alpha}{8\omega_0}r_0^2$$

to $O(\epsilon)$.

Magnetic field ripple in a dipole creates an additional force on the transverse motion of a particle. This is a time dependent force and acts every time the particle goes through the dipole. We assume for simplicity that there is magnetic ripple in only one dipole, placed at a phase ϕ_0. In one pass through the ring, the betatron phase ϕ advances by 2π radians. The equation of motion in the presence of ripple is,

$$\frac{d^2\xi}{d\phi^2} + \omega_0^2\xi + \epsilon\alpha\xi^3 = f(t)\sum_{m=-\infty}^{\infty}\delta(\phi - \phi_0 - 2\pi m) \quad . \tag{1.6}$$

Since the magnetic field ripple arises from current ripple in the power supplies, the time dependence of the ripple is of the form

$$f(t) = f_0 \cos\Omega_r t \quad ,$$

where Ω_r is the ripple frequency. We can expand the periodic delta function as

$$\sum_{m=-\infty}^{\infty}\delta(\phi - \phi_0 - 2\pi m) = \frac{1}{2\pi}\left[1 + 2\sum_{q=1}^{\infty}\cos q(\phi - \phi_0)\right] \quad .$$

For large rings and small non-linearities, the phase ϕ depends linearly on the time t as $\phi = \Omega_\beta t$, where Ω_β is the betatron frequency. Substituting these back into the equation of motion gives,

$$\frac{d^2\xi}{d\phi^2} + \omega_0^2\xi + \epsilon\alpha\xi^3 = \frac{1}{2\pi} f_0 \left[\cos\left(\frac{\Omega_r}{\Omega_\beta}\phi\right) + \sum_{q=1}^{\infty} \left\{ \cos\left[\left(\frac{\Omega_r}{\Omega_\beta} - q\right)\phi + q\phi_0\right] \right.\right.$$

$$\left.\left. + \cos\left[\left(\frac{\Omega_r}{\Omega_\beta} + q\right)\phi - q\phi_0\right] \right\} \right] \quad . \tag{1.7}$$

Of all the frequencies present in the forcing term on the right hand side, we pick that frequency which is closest to the betatron tune ω_0. Dropping all other terms, the equation of motion simplifies to

$$\frac{d^2\xi}{d\phi^2} + \omega_0^2\xi + \epsilon\alpha\xi^3 = \frac{1}{2\pi} f_0 \cos\Big[(\nu_0 + \epsilon\Delta)\phi + c_0\phi_0\Big] \quad , \tag{1.8}$$

where $\epsilon \ll 1$, and Δ is called the detuning. This is the equation for the forced Duffing oscillator without damping. In the event that there is significant ripple in N dipoles located at phases $\phi_j, j = 1, \ldots, N$, the above equation can be generalized to

$$\frac{d^2\xi}{d\phi^2} + \omega_0^2\xi + \epsilon\alpha\xi^3 = \frac{1}{2\pi} \sum_{j=1}^{N} f_j \cos\Big[(\nu_0 + \epsilon\Delta)\phi + c_j\phi_j\Big] \quad . \tag{1.9}$$

The questions of interest are

- What ripple frequencies Ω_r (or detunings Δ) lead to the largest beam emittance?
- In a typical accelerator ripple fields can always be reduced to low levels by properly designing the power supplies and also attaching appropriate filters to the magnets. However with a large number of magnets, even small ripple fields can lead to appreciable emittance growth over the lifetime of a beam. The question that arises is to what level must the ripple amplitudes f_j be reduced to avoid significant perturbation of the beam?

2. Collective behavior of driven linear oscillators

This section is a slightly generalized treatment of material that appears in [10]. It is included primarily for pedagogical reasons, to make clear the difference in behavior between an ensemble of linear oscillators and an ensemble of nonlinear oscillators.

We consider here the long time behavior of an ensemble of driven linear oscillators, each of which is governed by the equation of motion

$$\ddot{x} + \omega^2 x = F \cos\omega_r t \quad , \tag{2.1}$$

with initial conditions $x(0) = x_0$, $\dot{x}(0) = \dot{x}_0$. The general solution is

$$x(t) = x_0 \cos\omega t + \frac{\dot{x}_0}{\omega} \sin\omega t + \frac{F}{\omega^2 - \omega_r^2} \left[\cos\omega_r t - \cos\omega t\right] \quad , \tag{2.2}$$

which contains the special cases of linear growth for $\omega = 0$ and also $\omega^2 = \omega_r^2 \neq 0$ and quadratic growth for $\omega = \omega_r = 0$ in the usual limiting way. Here ensemble averages over x_0 and $\dot{x}_0$ have the same properties as the underlying dynamics, basically quasi-periodicity. To obtain non-trivial results consider an ensemble with a spread of natural frequencies ω, and distributed in phase space. For these linear oscillators the frequencies will, in general, be independent of the positions in phase space. In an accelerator this situation arises if the machine is perfectly linear but has non-zero chromaticity and the particles in the beam have a spread in energies. The density distribution describing the initial phase space coordinates $(x_0, \dot{x}_0)$ and the frequency for this ensemble can therefore be taken as a product distribution,

$$\rho(x_0, \dot{x}_0, \omega) = \rho_P(x_0, \dot{x}_0)\rho_f(\omega) \ , \tag{2.3}$$

which is normalized as

$$\int \rho_P(x_0, \dot{x}_0) dx_0 \, d\dot{x}_0 = 1 = \int \rho_f(\omega) \, d\omega \ . \tag{2.4}$$

Here, ρ_P and ρ_f denote the distributions in phase space and frequency respectively.

One might imagine that when the whole ensemble of particles is driven by the external force, the response of the resonant particles will be the most important in determining the position of the centroid. However the position of the centroid does not grow without limit at long times. This can be seen by computing the centroid position as the ensemble average of $x(t)$,

$$\Big\langle x(t) \Big\rangle = \int\int\int_{-\infty}^{\infty} x(t)\rho_P(x_0, \dot{x}_0)\rho_f(\omega) \, dx_0 d\dot{x}_0 d\omega \ . \tag{2.5}$$

The ensemble average can be written as a sum of two parts, the first depends on the initial conditions, the second on the response to the external force,

$$\Big\langle x(t) \Big\rangle = \langle x_0 \rangle \int \cos\omega t \rho_f(\omega) \, d\omega + \langle \dot{x}_0 \rangle \int \frac{\sin\omega t}{\omega} \rho_f \, d\omega + F \left\{ \int \frac{\rho_f(\omega)}{\omega^2 - \omega_r^2} \left[\cos\omega_r t - \cos\omega t\right] \, d\omega \right\} \ . \tag{2.6}$$

To calculate the average of the term in curly braces, we introduce the detuning parameter, $\Delta = \omega_r - \omega$. Substituting the single particle response given in Eq. (2.2) and changing the variable of integration to Δ gives

$$\Big\langle x(t) \Big\rangle = \langle x_0 \rangle \int \cos\omega t \rho_f(\omega) \, d\omega + \langle \dot{x}_0 \rangle \int \frac{\sin\omega t}{\omega} \rho_f \, d\omega \tag{2.7}$$

$$F \left[-\cos\omega_r t \int_{-\infty}^{\infty} \frac{\rho(\omega_r - \Delta)}{\Delta(2\omega_r - \Delta)} (\cos\Delta t - 1) \, d\Delta + \sin\omega_r t \int_{-\infty}^{\infty} \frac{\rho(\omega_r - \Delta)}{\Delta(2\omega_r - \Delta)} \sin\Delta t \, d\Delta \right] \ .$$

We are interested in the long time asymptotics of $\langle x(t)\rangle$. We use the following results

$$\lim_{t\to\infty} \frac{1-\cos\Delta t}{\Delta} = P.V.\left(\frac{1}{\Delta}\right)$$

$$\lim_{t\to\infty} \frac{\sin\Delta t}{\Delta} = \pi\delta(\Delta)$$

where $P.V.$ indicates the Cauchy principal value of an integral. The above equalities are to be understood as being applied to distributions. Using these equalities, we obtain

$$\Big\langle x(t)\Big\rangle \sim \langle x_0\rangle \int \cos\omega t \rho_f(\omega)\, d\omega + \pi\langle \dot{x}_0\rangle \rho_f(0)$$

$$+F\left[-\cos\omega_r t\ P.V. \int_{-\infty}^{\infty} \frac{\rho(\omega_r-\Delta)}{\Delta(2\omega_r-\Delta)}\, d\Delta + \pi\sin\omega_r t \frac{\rho(\omega_r)}{2\omega_r}\right] \quad , \tag{2.8}$$

as $t \to \infty$. By the Riemann-Lebesgue lemma which says that if f is absolutely integrable, then $\int_{-\infty}^{\infty} f(x)e^{itx}dx \to 0$ as $|t| \to \infty$ (see e.g. [11]), it follows that in the limit the first term vanishes and for a phase space distribution symmetric about the origin, $\langle \dot{x}_0\rangle = 0$. Thus we are left with only the response to the external force. We can assume that $\rho(\omega)$ is sharply peaked at some frequency $\bar{\omega}$ which is near ω_r, i.e. $\rho(\omega_r-\Delta)$ is non-zero only for $\Delta << \omega_r$. This amounts to saying that the external drive force is nearly resonant with the core of the particles in the ensemble. This approximation enables us to simplify the result for the position of the centroid to

$$\langle x(t)\rangle = \frac{F}{2\omega_r}\left[\cos\omega_r t\ P.V. \int_{-\infty}^{\infty} \frac{\rho_f(\omega)}{\omega-\omega_r}\, d\omega + \pi\sin\omega_r t\ \rho_f(\omega_r) + o(1)\right] \quad , \tag{2.9}$$

as $t \to \infty$. This expression shows that at long times, the centroid oscillates at the external drive frequency with a finite amplitude. This lack of growth in the centroid motion in the presence of an external force is also known as Landau damping [10].

The average amplitude of the ensemble in phase space (or equivalently the energy) does however grow in time by absorbing energy from the external source. This can be seen by calculating the long time asymptotics of $\langle x^2\rangle$. We proceed as before and for the evaluation of the asymptotics we need the following results:

$$\lim_{t\to\infty} \frac{1-\cos\Delta t}{\Delta^2} = \lim_{t\to\infty} \pi\delta(\Delta)t \ ,$$

$$\lim_{t\to\infty} \frac{1-2\cos\Delta t+\cos 2\Delta t}{\Delta^2} = -\frac{d}{d\Delta}P.V.\left(\frac{1}{\Delta}\right) \ ,$$

$$\lim_{t\to\infty} \frac{\sin 2\Delta t - 2\sin\Delta t}{\Delta^2} = \frac{\pi}{2}\frac{d}{d\Delta}\delta(\Delta) \ ,$$

$$\lim_{t\to\infty} \frac{\sin 2\Delta t - \sin\Delta t}{\Delta} = 0 = \lim_{t\to\infty} \frac{\cos 2\Delta t - \cos\Delta t}{\Delta} \ . \tag{2.10}$$

These results can be derived by taking the Fourier transform of the expression on the left hand side with respect to Δ, evaluating the long time limit and then taking the inverse transform. Using these equalities, integrating by parts and making use of the Riemann-Lebesgue lemma,

$$\begin{aligned}\left\langle x^2(t)\right\rangle \sim & \frac{1}{2}\langle x_0^2\rangle + \pi\langle \dot{x}_0^2\rangle \rho_f(0)t + \pi\langle x_0\dot{x}_0\rangle \rho_f(0) \\ & + F\langle x_0\rangle P.V.\int_{-\infty}^{\infty} \frac{\rho_f(\omega_r-\Delta)}{\Delta(2\omega_r-\Delta)}\, d\Delta + \frac{F\langle \dot{x}_0\rangle}{\omega_r^2}\rho_f(0)(1-2\cos\omega_r t) \\ & + F^2\left\{\frac{\pi\rho_f(\omega_r)}{4\omega_r^2}t + \frac{1}{2}\cos 2\omega_r t P.V.\int_{-\infty}^{\infty}\frac{1}{\Delta}\frac{d}{d\Delta}\left[\frac{\rho_f(\omega_r-\Delta)}{(2\omega_r-\Delta)^2}\right] d\Delta \right. \\ & \left. - \frac{\pi}{2}\sin 2\omega_r t \frac{d}{d\Delta}\left[\frac{\rho_f(\omega_r-\Delta)}{(2\omega_r-\Delta)^2}\right]\Bigg|_{\Delta=0}\right\} \quad , \end{aligned} \tag{2.11}$$

as $t \to \infty$. For symmetric phase space distributions the terms in the second line vanish. Keeping only the dominant terms shows that the growth of $\langle x^2(t)\rangle$ is linear in time,

$$\langle x^2(t)\rangle = \pi\left[\langle \dot{x}_0^2\rangle \rho_f(0) + \frac{F^2}{4\omega_r^2}\rho_f(\omega_r)\right] t + O(1) \tag{2.12}$$

at long times. Thus we see that the density of free particles ($\omega = 0$) and exactly resonant particles ($\omega = \omega_r$) determines the long time behavior of the ensemble. For these particles, x^2 grows as t^2. However in averaging over the ensemble we include particles nearby in frequency for which the motion is only oscillatory. This slows the collective behavior of the ensemble by one power of t.

In the rest of the paper we consider the nonlinear case where we will see that the averages are bounded and the linear growth in time does not hold.

3. Numerical solution of the Duffing equation

3.1. Single particle behavior

A single undamped driven Duffing oscillator is described by the equation

$$\ddot{x} + \omega_0^2 x + \epsilon\alpha x^3 = \epsilon f\cos(\omega_r t + \phi) \ , \tag{3.1}$$

where ω_0 is the natural frequency of the oscillator in the absence of non-linearities and external forcing. Both the non-linearity and the external force are assumed small : $0 < \epsilon \ll 1$. The assumption of a small force precludes the existence of chaotic behavior in most of phase space. We allow for an arbitrary initial phase ϕ of the force. This phase affects the short time behavior of the particle but not the behavior at long times.

The response of the particle can be described by the Fourier modes in x. The amplitudes and frequencies of these modes depend on the parameters in the equation of motion and also on the initial conditions. The restriction to small forcing limits the number of significant Fourier modes.

In fig. 1 we show a $2\pi/\omega_r$ Poincaré section for 3 particles over a hundred periods of the external force. In figs. 2, 3 and 4 are shown their Fourier spectra. Particle 1 which is practically stationary in the Poincaré plot has one significant Fourier mode at the drive frequency ω_r, particle 2 with a greater excursion in phase space has three significant nearly equally spaced modes (one at ω_r) while particle 3 whose motion is symmetric about both $(x, \dot{x})$ axes again has only one significant mode. The dependence of the Fourier spectra on the initial conditions will be explained in Section 4.5.

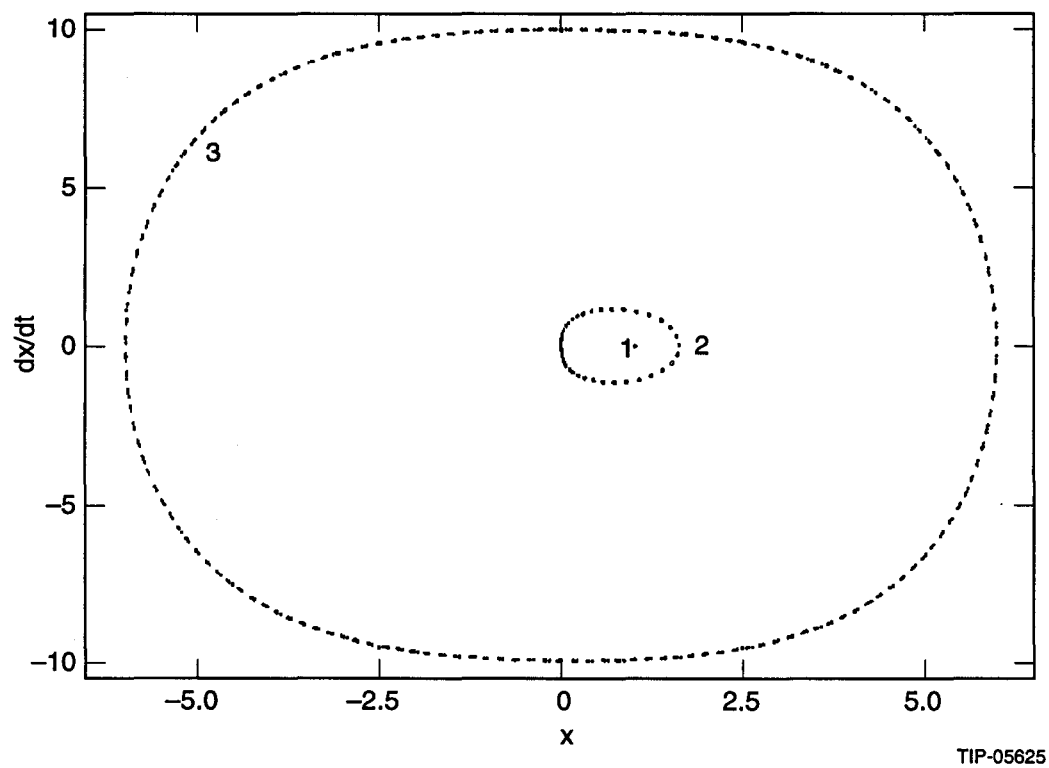

Fig. 1. Poincaré plot over 500 periods of 3 particles; ϵ=0.1, $\alpha = 1.0$, f=1.0, $\omega_0 = 1.0$, $\omega_r = 0.99$.

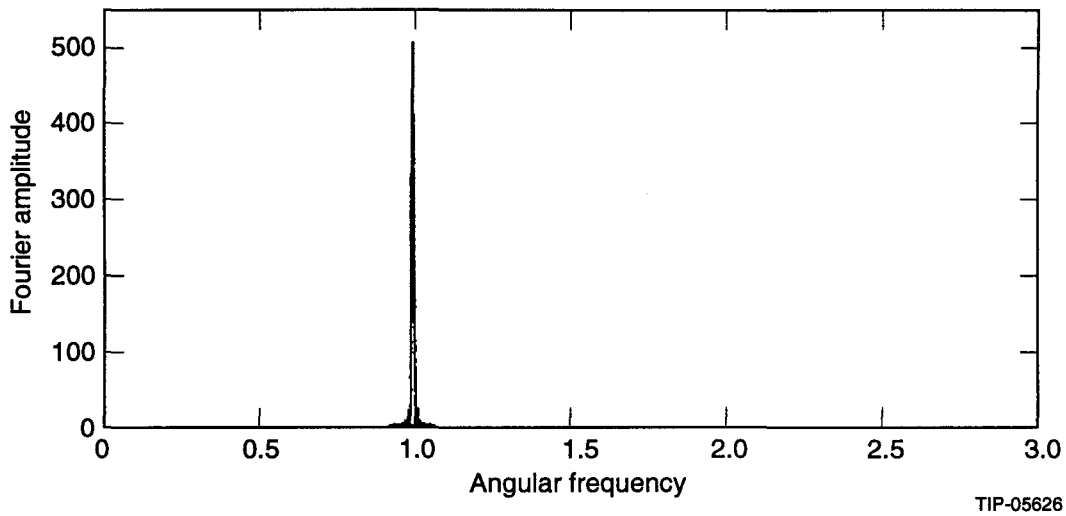

Fig. 2. Fourier spectrum of particle 1 in fig. 1 with largest peak at $\omega = \omega_r = 0.99$, the drive frequency; ϵ=0.1, $\alpha = 1.0$, f=1.0, $\omega_0 = 1.0$.

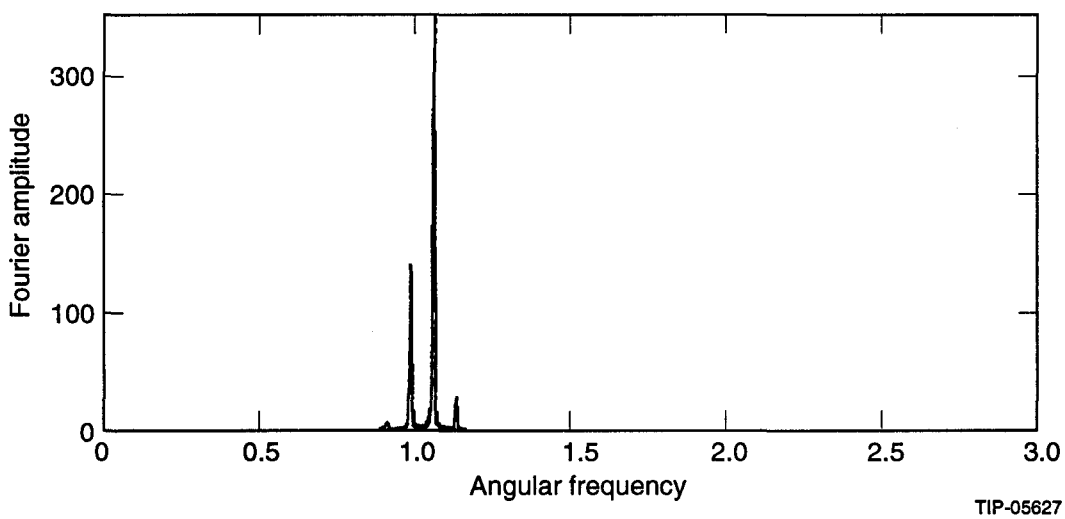

Fig. 3. Fourier spectrum of particle 2 in fig. 1 with largest peak at $\omega = 1.29$; ϵ=0.1, $\alpha = 1.0$, f=1.0, $\omega_0 = 1.0$, $\omega_r = 0.99$.

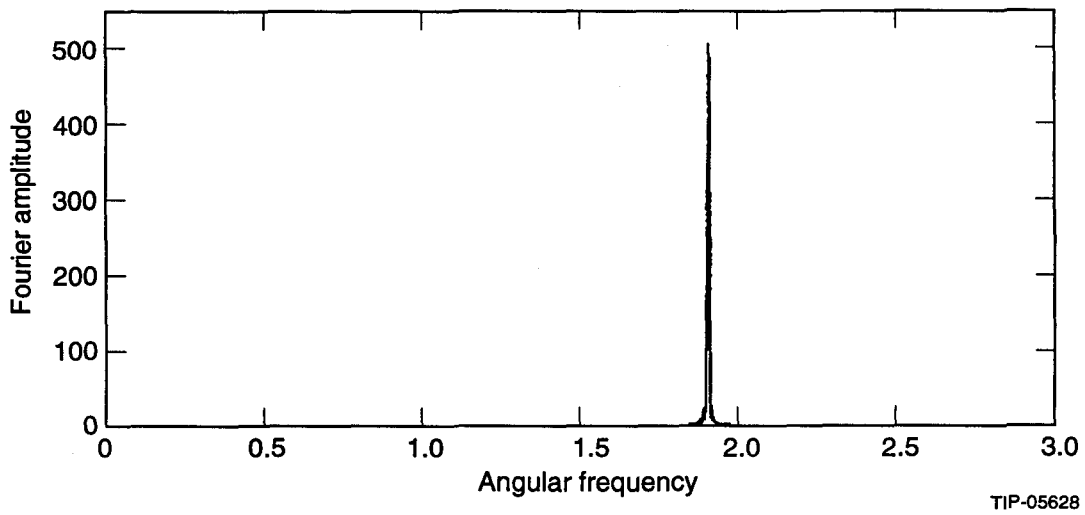

Fig. 4. Fourier spectrum of particle 3 in fig. 1 with largest peak at $\omega = 1.89$; ϵ=0.1, $\alpha = 1.0$, f=1.0, $\omega_0 l = 1.0$, $\omega_r = 0.99$.

3.2. Time evolution of the averaged amplitude

Our main aim in this paper is to understand the collective behavior of an ensemble of Duffing oscillators with application to the motion of particles in a storage ring. The initial distribution of particles in phase space changes in time due to the forces acting on them. We wish to follow this evolution in time and determine the change in the size of the distribution. In this section we will do so by numerical integration of the equations of motion. In proton storage rings the particle distribution is well approximated by a Gaussian distribution in phase space. For the numerical simulations reported here, we take a total of 10^4 particles distributed as a bi-Gaussian in $(x, \dot{x})$ space with a unit variance in each and a zero covariance. We use the integrator RKF45 [12] in double precision with an error tolerance of 10^{-7}. Decreasing the error tolerance to 10^{-8} changes the values at long times only by one part in a thousand.

It was mentioned in Section 1 that the questions of interest are the effects on the distribution size as we change the parameters of the time periodic force—the amplitude f and the frequency ω_r. We will examine the case when the external frequency is close to the linearized frequency of the particles and thus we define the detuning parameter Δ as

$$\omega_r = \omega_0 + \epsilon\Delta \ . \tag{3.2}$$

Here we will show representative examples of these effects as found by the numerical integration. We consider the following quantity as a measure of the size of the distribution in phase space,

$$\langle A^2 \rangle = \left\langle x^2 + \frac{1}{\omega_r^2}\dot{x}^2 \right\rangle \tag{3.3}$$

where $\langle\rangle$ denotes the average over all particles. It turns out to be more convenient (as will be seen in Section 8) to consider A^2 rather than $x^2 + \dot{x}^2/\omega_0^2$, although ω_0, ω_r are close. We calculate the time evolution of $\langle A^2 \rangle$ and write out its value every period of the force so that we are viewing $\langle A^2 \rangle$ in a Poincaré section. Figures 5 and 6 show the time evolution for the same amplitude of the force ($f = 1.0$) but different detunings. Figure 7 shows the evolution at a larger force ($f = 10.0$) and the same detuning as in fig. 5.

All three figures show that $\langle A^2 \rangle$ rises quickly to a peak value and then performs smaller amplitude oscillations about a value to which it relaxes at long times. This is to be contrasted with the behavior of an ensemble of driven linear oscillators for which $\langle A^2 \rangle$ grows linearly with time. A comparison of figs. 5 and 6 shows that it takes longer to equilibrate at the lower value of the detuning if the force is held constant. From figs. 5 and 7 we observe that, with the detuning kept constant, both the final equilibrium value and the frequency of oscillations increase nonlinearly with the forcing amplitude. We will explain these observations by a theoretical analysis in the subsequent sections.

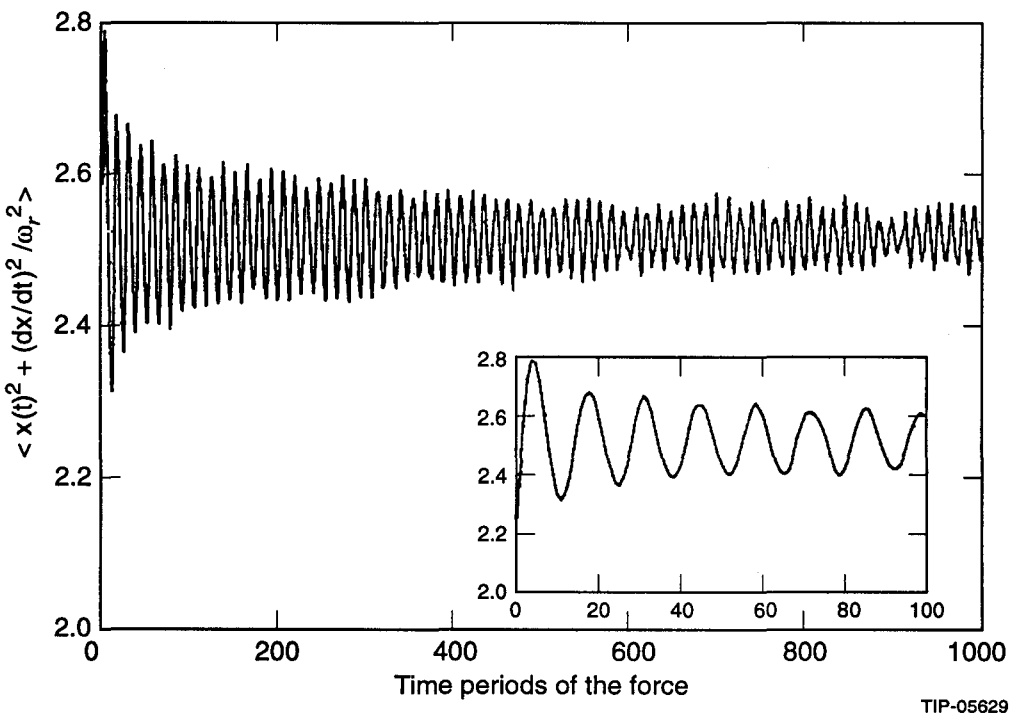

Fig. 5. Time evolution of the ensemble average$< x^2 + (\dot{x}/\omega_r)^2 >$ in a Poincaré section for a Gaussian distribution with 10^4 particles; ϵ=0.1, $\alpha = 1.0$, f=1.0, $\omega_0 = 1.0$, $\Delta = -0.1$. The inset shows the evolution over 100 periods.

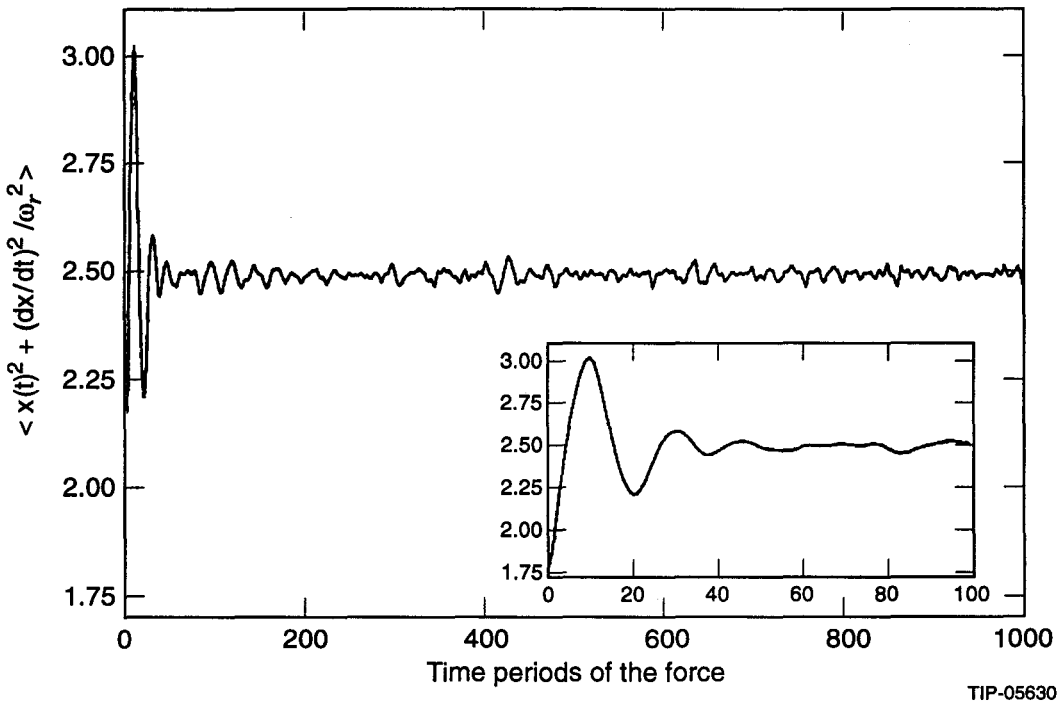

Fig. 6. Same as fig. 5 but a different detuning:$\Delta = 2.0$.

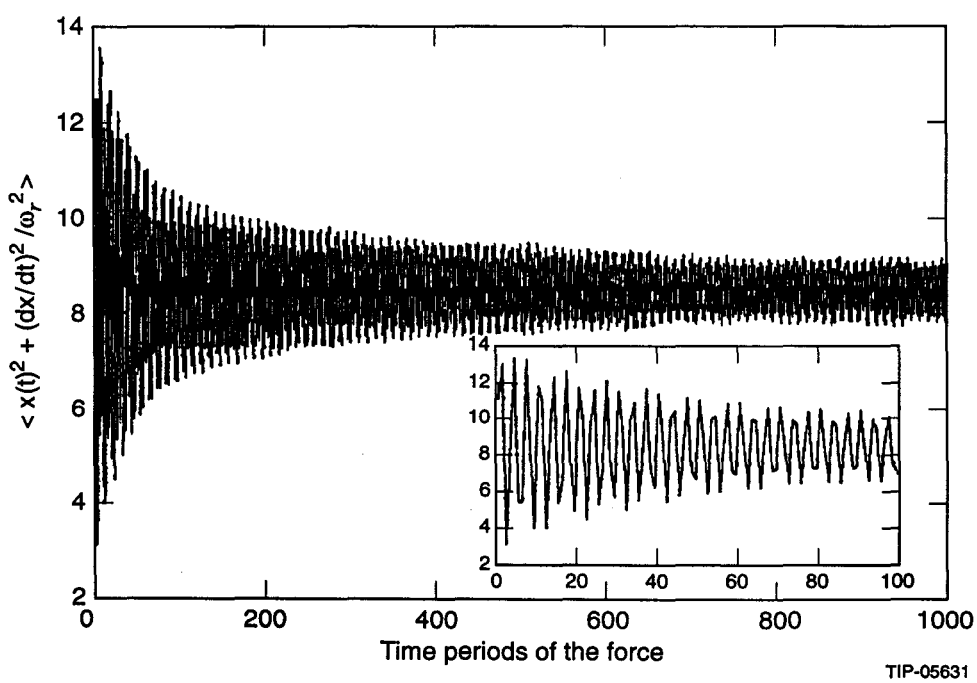

Fig. 7. Same as fig. 5 but a different force: f=10.0.

4. The averaging approximation

4.1. The averaging theorem

Consider the undamped, driven Duffing oscillator,

$$\ddot{x} + \omega_0^2 x + \epsilon\alpha x^3 = \epsilon f \cos(\omega_r t + \phi) \tag{4.1}$$

with small forcing and small nonlinearity, i.e. $\epsilon \ll 1$. Let

$$\tau = \omega_r t \ , \ \omega_r = \omega_0 + \epsilon\Delta \tag{4.2}$$

and notice that we are near the 1:1 resonance with Δ the resonance parameter. The equivalent system of first order ODEs,

$$\begin{aligned} \frac{d}{d\tau}x_1 &= x_2 \\ \frac{d}{d\tau}x_2 &= -x_1 + \frac{\epsilon}{\omega_0}\left(2\Delta x_1 - \alpha\frac{x_1^3}{\omega_0} + \frac{f}{\omega_0}\cos\tau\right) + O(\epsilon^2) \end{aligned} \tag{4.3}$$

can be written as

$$\frac{d}{d\tau}\mathbf{x} = J\mathbf{x} + \epsilon\mathbf{g}(\mathbf{x},\tau) + \epsilon^2\mathbf{h} \ , \qquad \mathbf{x}(\tau_0) = \mathbf{x}_0 \tag{4.4}$$

where $\mathbf{x} = (x, \dot{x}) \equiv (x_1, x_2)$ and J is the symplectic matrix. This can be transformed to a standard form for the method of averaging by

$$\mathbf{x} = e^{J(\tau-\tau_0)}\mathbf{y} \ , \tag{4.5}$$

which yields

$$\frac{d}{d\tau}\mathbf{y} = \epsilon e^{-J(\tau-\tau_0)}\mathbf{g}\left(e^{J(\tau-\tau_0)}\mathbf{y},\tau\right) + O(\epsilon^2) \equiv \epsilon\mathbf{G}(\mathbf{y},\tau,\tau_0) + O(\epsilon^2) \ , \quad \mathbf{y}(\tau_0) = \mathbf{x}_0 \ . \tag{4.6}$$

Here τ_0 is inserted in (4.5) so that in the τ_0 Poincaré section, $\mathbf{x} = \mathbf{y}$. The vector field $\mathbf{G}$ is 2π periodic in τ and the first order Averaging Theorem, as presented in Appendix A, states that

$$\mathbf{y}(\tau) = \mathbf{u}(\tau) + \epsilon\mathbf{P}\Big(\mathbf{u}(\tau),\tau,\tau_0\Big) + O\Big(\epsilon^2(\tau-\tau_0)\Big) \tag{4.7}$$

for $0 \le \tau \le T/\epsilon$. Thus $\mathbf{P}$ increases the accuracy at $O(1)$ times but not at $O(1/\epsilon)$. Here

$$\mathbf{P}(\mathbf{u},\tau,\tau_0) = \int_{\tau_0}^{\tau}\Big[\mathbf{G}(\mathbf{u},\tau,\tau_0) - \bar{\mathbf{G}}(\mathbf{u},\tau_0)\Big]\,d\tau \tag{4.8}$$

is 2π periodic in τ and $\mathbf{u}$ satisfies the averaged equation,

$$\frac{d\mathbf{u}}{d\tau} = \epsilon\bar{\mathbf{G}}(\mathbf{u},\tau_0), \qquad \bar{\mathbf{G}}(\mathbf{u},\tau_0) = \frac{1}{2\pi}\int_0^{2\pi}\mathbf{G}(\mathbf{u},\tau,\tau_0)\,d\tau \ , \quad \mathbf{u}(\tau_0) = \mathbf{x}_0 \ . \tag{4.9}$$

If we let

$$\kappa = \frac{f}{2\omega_0} \quad , \quad \lambda = \frac{3\alpha}{8\omega_0} \quad . \tag{4.10}$$

then $\bar{\mathbf{G}}$ is found to be

$$\bar{\mathbf{G}} = \frac{1}{\omega_0} \begin{bmatrix} -\Delta v + \lambda(u^2+v^2)v + \kappa \sin(\tau_0 + \phi) \\ \Delta u - \lambda(u^2+v^2)u + \kappa \cos(\tau_0 + \phi) \end{bmatrix} \quad , \tag{4.11}$$

where $\mathbf{u} = (u, v)$. Furthermore (4.9) can be obtained from the Hamiltonian

$$\frac{\omega_0}{\epsilon}\tilde{H} = -\frac{\lambda}{4}(u^2+v^2)^2 + \frac{\Delta}{2}(u^2+v^2) - \kappa \sin(\tau_0+\phi)v + \kappa\cos(\tau_0+\phi)u \tag{4.12}$$

with

$$\frac{d}{d\tau}u = -\frac{\partial \tilde{H}}{\partial v} \quad , \quad \frac{d}{d\tau}v = \frac{\partial \tilde{H}}{\partial u} \quad .$$

It turns out that $\bar{\mathbf{G}}$ is such that all solutions of (4.9) exist for all time and that T can be any positive constant. It follows from (4.5) and (4.7) that

$$\begin{aligned} \mathbf{x}(\tau) &= e^{J(\tau-\tau_0)}\mathbf{u} + O(\epsilon) \\ &= \begin{bmatrix} \cos(\tau-\tau_0)u + \sin(\tau-\tau_0)v \\ -\sin(\tau-\tau_0)v + \cos(\tau-\tau_0)u \end{bmatrix} + O(\epsilon) \quad , \end{aligned} \tag{4.13}$$

for $0 \le \tau - \tau_0 \le T/\epsilon$ .On a τ_0 Poincaré section

$$\mathbf{x}(\tau_0 + 2n\pi) = \mathbf{u}(\tau_0 + 2n\pi) + O(\epsilon^2 n) \qquad \text{for } 0 < 2n\pi < T/\epsilon \quad . \tag{4.14}$$

It is interesting to note that $\mathbf{u}$ thus defines the Poincaré map with an accuracy of $O(\epsilon^2)$, a fact we will not make use of in this paper. From Eq. (4.13), it is clear that $\mathbf{u}$ describes the slow oscillations of the envelope of $\mathbf{x}$.

To analyze the averaged equations, we first find the equilibrium points and analyze their stability. We then construct the phase plane portraits. At a later stage we will find the solution in terms of elliptic functions.

It should be emphasized that these results are valid on time intervals of $O(1/\epsilon)$ and we hope that this is long enough for equilibrium to set in. We do not expect $\mathbf{u}(\tau)$ to give a good approximation on longer intervals because in general we expect the $\mathbf{u}$ motion to become out of phase with the $\mathbf{y}$ motion at longer times. However we can say something at longer times because the adiabatic invariant results developed in [13] can be applied. They show that Hamiltonians such as the one in (4.12) when evaluated along the solution $y(t)$ or along $x(t)$ in the τ_0 section cannot change significantly until times of $O(1/\epsilon^2)$. Since our equilibrium results really only need motion on an energy surface, this may mean that averaging results work on longer intervals.

4.2. Fixed points of the averaged equations and their stability

To obtain simple equations for finding the fixed points we define the polar variables (a, γ) as,

$$u = a\cos(\gamma - \tau_0 - \phi)$$
$$v = a\sin(\gamma - \tau_0 - \phi) \tag{4.15}$$

where $a \geq 0$. At this point we set the section time τ_0 and the initial phase ϕ to zero. The initial phase ϕ affects only the transient behavior of the particles and not the long time behavior, our focus of interest. The section time affects the orientation of the Poincaré map but not the ensemble averages of rotationally invariant quantities such as $u^2 + v^2$. The fixed points (a_c, γ_c) are then determined by setting $\bar{\mathbf{G}} = 0$ to zero which leads to the equations

$$\sin\gamma_c = 0 \ , \tag{4.16}$$

$$f(a_c) \equiv \lambda a_c^3 - \Delta a_c - \kappa\cos\gamma_c = 0 \ . \tag{4.17}$$

The first equation leads to the two possibilities $\gamma_c = 0,\ \pi$. Since $f'(a) = 0$ for $a = \pm\sqrt{\Delta/3\lambda}$, there are three real roots if $f(-\sqrt{\Delta/3\lambda}) > 0$, i.e. if

$$\Delta > \Delta_{bf} \equiv 3\left[\frac{\lambda\kappa^2}{4}\right]^{1/3} \tag{4.18}$$

and there is only one real root if the detuning $\Delta < \Delta_{bf}$. For $\Delta > \Delta_{bf}$ we define

$$\theta(\gamma_c) = \frac{1}{3}\cos^{-1}\left[\left(\frac{\Delta_{bf}}{\Delta}\right)^{3/2}\cos\gamma_c\right] \quad , \quad 0 < 3\theta < \pi \ .$$

Choosing the positive values of a from the six possibilities gives three fixed points at

$$a_1 = 2\sqrt{\frac{\Delta}{3\lambda}}\cos\Big[\theta(0)\Big] \tag{4.19}$$

$$a_2 = 2\sqrt{\frac{\Delta}{3\lambda}}\cos\left[\frac{4\pi}{3} + \theta(\pi)\right] \tag{4.20}$$

$$a_3 = 2\sqrt{\frac{\Delta}{3\lambda}}\cos\Big[\theta(\pi)\Big] \ . \tag{4.21}$$

These fixed points are ordered as

$$0 < a_2 < \sqrt{\Delta/(3\lambda)} < a_3 < \sqrt{\Delta/\lambda} < a_1 \ .$$

In the (u, v) phase space, the three fixed points are at $(u_{c1}, v_{c1}) = (a_1, 0)$, $(u_{c2}, v_{c2}) = (-a_2, 0)$ and $(u_{c3}, v_{c3}) = (-a_3, 0)$.

If $\Delta < \Delta_{bf}$, then the single positive real root of the cubic is

$$a_0 = \sqrt{\frac{\Delta_{bf}}{3\lambda}} \left(\left[1 + \sqrt{1 - \left(\frac{\Delta}{\Delta_{bf}}\right)^3} \right]^{1/3} + \left[1 - \sqrt{1 - \left(\frac{\Delta}{\Delta_{bf}}\right)^3} \right]^{1/3} \right) . \tag{4.22}$$

The fixed point is at $(u_{c0}, v_{c0}) = (a_0, 0)$. At the bifurcation point $\Delta = \Delta_{bf}$ there are two equilibrium points, one at $a_1 = 2\sqrt{\frac{\Delta_{bf}}{3\lambda}}$ and the other at $a_2 = a_3 = a_1 \cos \pi/3$.

In fig. 8 we show how the amplitudes of these fixed points vary with the detuning Δ.

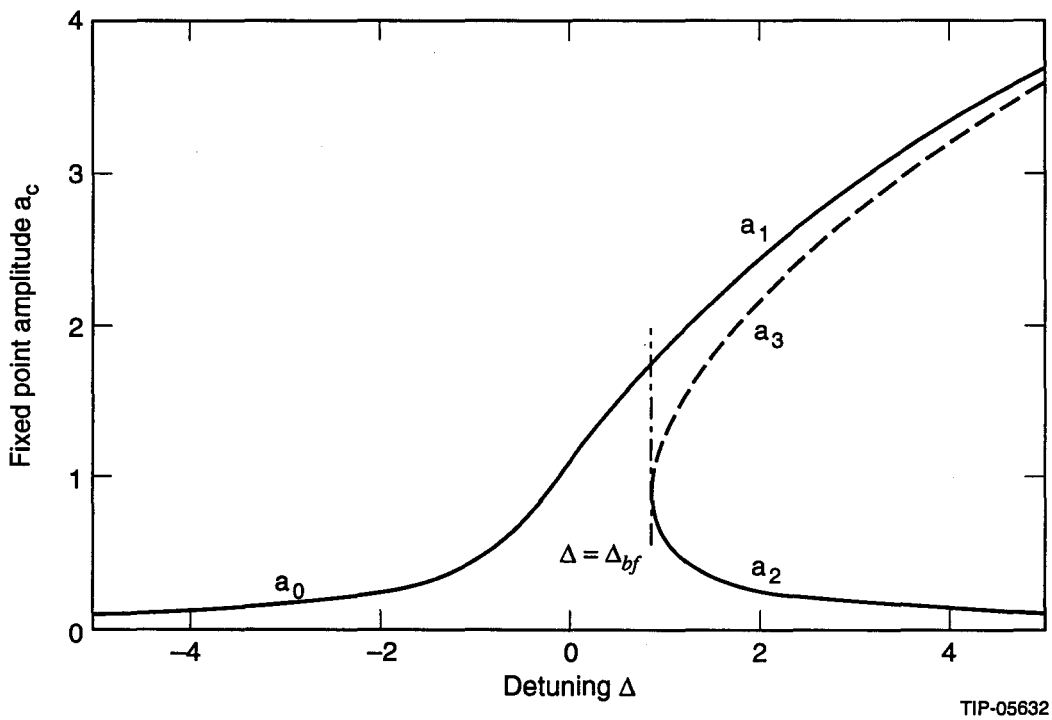

Fig. 8. Fixed points as a function of the detuning; $\lambda = 3/8$, $\kappa = 0.5$.

We now examine the stability of small amplitude motions around these fixed points. The Jacobian matrix is

$$D\bar{\mathbf{G}}(\mathbf{u}, \tau_0)|_{\mathbf{u}=\mathbf{u}_c} = \begin{bmatrix} 0 & -\Delta + 3\lambda a_c^2 \\ \Delta - \lambda a_c^2 & 0 \end{bmatrix} . \tag{4.23}$$

The stability eigenvalues μ are thus given by

$$\mu = \pm i \sqrt{[\lambda a_c^2 - \Delta]\,[3\lambda a_c^2 - \Delta]} . \tag{4.24}$$

Thus for $\mu \neq 0$ the equilibrium is unstable for μ real and linearly stable for μ imaginary. The fact that linear stability implies stability follows from the Hamiltonian structure. $\lambda a_c^2 - \Delta \neq 0$ if $\kappa \neq 0$

but if $3\lambda a_c^2 - \Delta = 0$, then two roots coalesce and a phase plane analysis shows that the fixed point is unstable.

For $\Delta > \Delta_{bf}$, the stable fixed points are at $(a_1, 0)$, $(-a_2, 0)$ while the fixed point at $(-a_3, 0)$ is unstable. For $\Delta < \Delta_{bf}$, the fixed point at $(a_0, 0)$ is stable. The frequency of small amplitude oscillations about a stable fixed point is $\Omega_c = \sqrt{(\lambda a_c^2 - \Delta)(3\lambda a_c^2 - \Delta)}$. Figure 9 shows that Ω_c around a_0 decreases as Δ approaches zero from below, then increases slowly till $\Delta \to \Delta_{bf}$. At the bifurcation point $\Delta = \Delta_{bf}$, $\Omega_c = \Delta_{bf}$. The fixed point a_0 becomes the fixed point a_1 for $\Delta > \Delta_{bf}$ and the frequency around a_1 also increases slowly with Δ. The fixed point at a_2 is closest to the origin and it moves in rapidly towards the origin as Δ increases beyond Δ_{bf}. The frequency of small amplitude motion around a_2 grows with corresponding rapidity as Δ increases (around a_2, $\Omega_c \approx \Delta$ for large Δ).

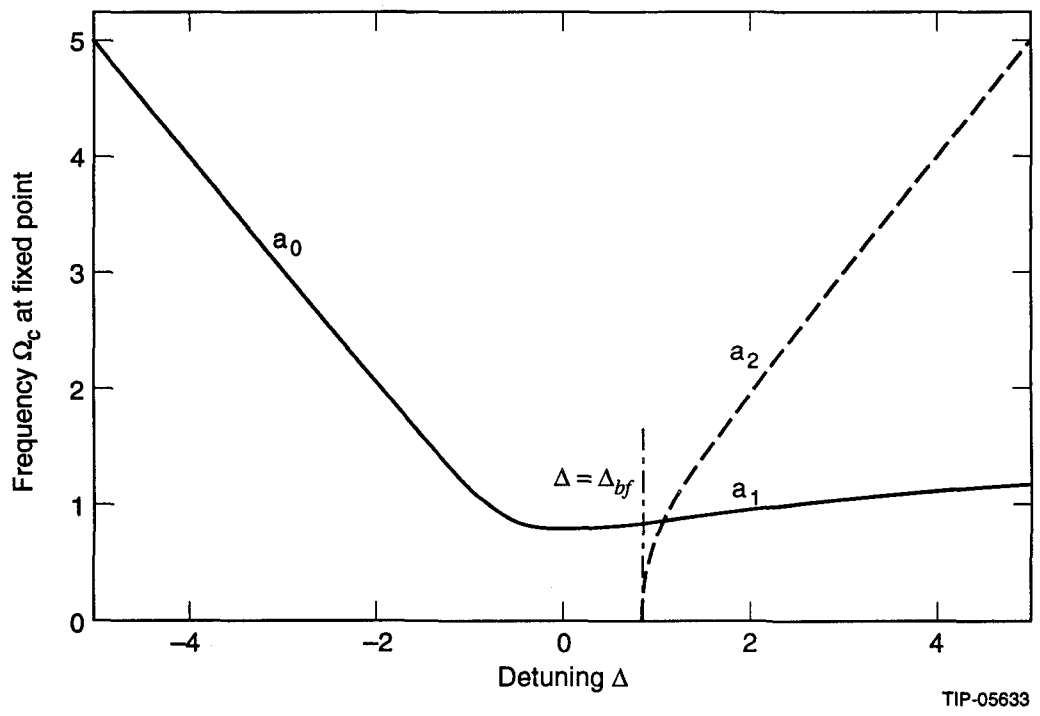

Fig. 9. Frequency at stable fixed points vs. the detuning; $\lambda = 3/8$, $\kappa = 0.5$.

4.3. Phase plane portraits

Define the slow time variable $\eta = \epsilon\tau/\omega_0$ and let a prime denote a derivative with respect to η. Then from (4.9) and (4.11) it follows that

$$u' = -\frac{\partial H}{\partial v} = -\Delta v + \lambda(u^2 + v^2)v \tag{4.25}$$

$$v' = \frac{\partial H}{\partial u} = \kappa + \Delta u - \lambda(u^2 + v^2)u \tag{4.26}$$

where

$$H = -\frac{\lambda}{4}(u^2 + v^2)^2 + \frac{\Delta}{2}(u^2 + v^2) + \kappa u \ . \tag{4.27}$$

Furthermore, the Hamiltonian is symmetric in v, so that the phase curves in the (u, v) plane are symmetric about the u axis and we can describe the phase curves by $v(u, E) \geq 0$ where $H(u, v(u, E)) = E$.

To determine v we define

$$R = \sqrt{u^2 + v^2} \geq 0 \tag{4.28}$$

and note that $H = -\frac{\lambda}{4}R^4 + \frac{\Delta}{2}R^2 + \kappa u$. Thus

$$R^2(u, E) = \frac{\Delta}{\lambda} \pm \frac{2}{\lambda}\sqrt{\lambda\Big((\kappa u) - E\Big) + \frac{\Delta^2}{4}} \ , \tag{4.29}$$

$$v(u, E) = \pm\sqrt{R^2 - u^2} \ . \tag{4.30}$$

For later use we note that (for $v \geq 0$),

$$\frac{\partial v}{\partial E} = -\frac{1}{(\lambda R^2 - \Delta)\sqrt{R^2 - u^2}} \tag{4.31}$$

and the opposite sign in the lower half of the phase plane.

The shape of the equal energy contours depends on whether Δ is less than or greater than 0. For $\Delta < 0$, only the positive sign in the expression for R^2 leads to positive values of R^2. This also implies that v is a single valued function of u over all of phase space. For $\Delta > 0$ however, both signs in the solution for R are allowed but in different regions of phase space. As a consequence, v is not a single valued function of u and the phase portrait has folds in it. The turning points in the phase portrait occur where the slope of v becomes infinite and dv/du is infinite when the right hand side of (4.25) is zero, thus either $v = 0$ or $\lambda R^2 - \Delta = 0$. The latter gives

$$u = u_{turn} \equiv \frac{1}{\kappa}\Big[E - \Delta^2/(4\lambda)\Big] \ .$$

At $u = u_{turn}$, the sign of the square root in the expression for R^2 changes sign and $R^2 = \Delta/\lambda$. Thus all turning points (not on the u axis) for the kidney shaped equal energy contours lie on a circle of radius $\sqrt{\Delta/\lambda}$. Particles which have such turning points have energies E in the range

$$E_{low} \equiv \frac{\Delta^2}{4\lambda} - \kappa\sqrt{\frac{\Delta}{\lambda}} \leq E \leq \frac{\Delta^2}{4\lambda} + \kappa\sqrt{\frac{\Delta}{\lambda}} \equiv E_{high} \ . \tag{4.32}$$

For all particles in this energy range, the turning points in u are at $u_{min}, u_{turn}, u_{max}$ with $u_{turn} \leq u_{min} \leq u_{max}$. Travelling along a contour from u_{min} to u_{turn},

$$R^2 = R_-^2 = \frac{\Delta}{\lambda} - \frac{2}{\lambda}\sqrt{\lambda\Big((\kappa u(t) - E\Big) + \frac{\Delta^2}{4}}$$

and from u_{turn} to u_{max}

$$R^2 = R_+^2 = \frac{\Delta}{\lambda} + \frac{2}{\lambda}\sqrt{\lambda\Big(\kappa u(t) - E\Big) + \frac{\Delta^2}{4}} \ .$$

Outside this energy range we take the positive sign for all contours. We now construct several phase plane portraits.

1. $\Delta < \Delta_{bf}$

The energy E is bounded from above, it takes on the maximum value E_{max} at the fixed point $(u_{c0}, v_{c0}) = (a_0, 0)$, this value is

$$E_{max} = -\frac{\lambda}{4}u_{c0}^4 + \frac{\Delta}{2}u_{c0}^2 + \kappa u_{c0} \ . \tag{4.33}$$

At the origin of phase space, E vanishes.

Figure 10 shows the phase curves in (u, v) space for a few values of the energy at at detuning far below the bifurcation value $\Delta_{bf} \approx 0.859$. Figure 11 shows the phase portrait at a detuning $\Delta = 0.75$ much closer to the bifurcation value. In either case, for $E \ll 0$ the phase curves are approximately circles given by $R^2 = \sqrt{-4E/\lambda}$, as is seen from (4.27).

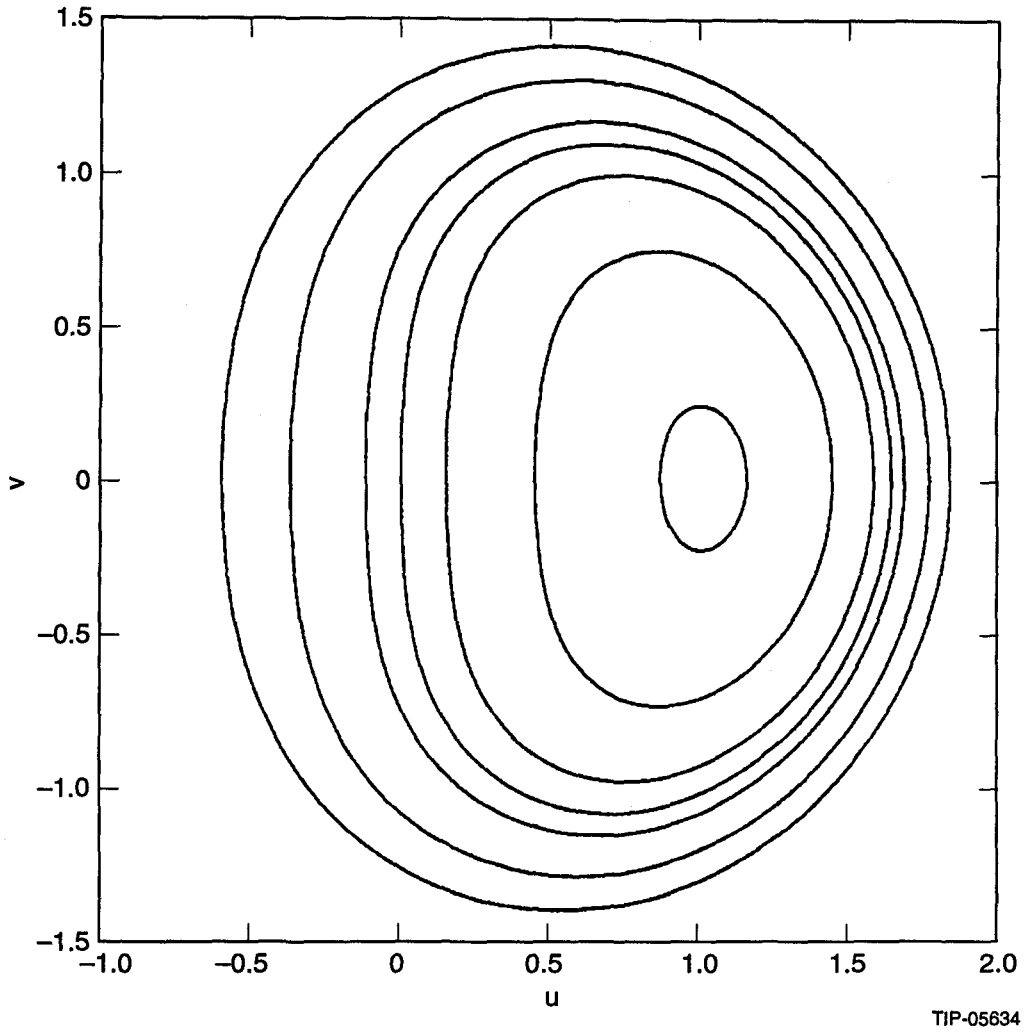

Fig. 10. Equal energy contours in (u, v) phase space below the bifurcation value of Δ: $\lambda = 3/8$, $\kappa = 0.5$, $\Delta = -0.1$. The bifurcation value is $\Delta_{bf} \approx 0.859$. The fixed point is at (u_{c0}, v_{c0})=(1.020,0.0).

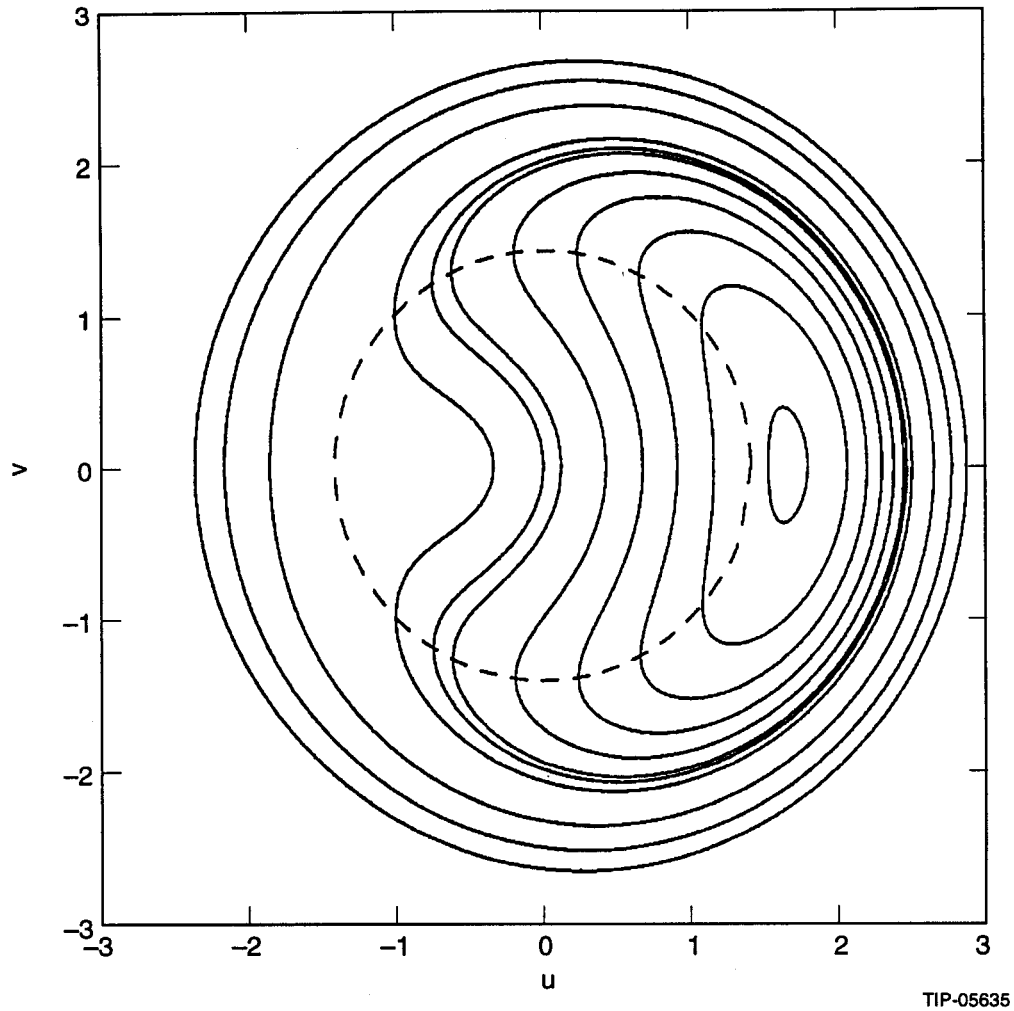

Fig. 11. Same as fig. 10 except that $\Delta = 0.75$. The dotted lines show the circle of radius $[\Delta/\lambda]^{1/2}$ on which the turning points (off the u axis) lie. The fixed point is at $(u_{c0}, v_{c0}) = (1.672, 0.0)$.

2. $\Delta > \Delta bf$

In this case the two stable fixed points are at amplitudes a_1, a_2 and the unstable fixed point is at an amplitude a_3, these being ordered as $0 < a_2 < a_3 < a_1$. The corresponding energies are ordered as $E[a_2] < E[a_3] < E[a_1]$. Note that the energy has a global maximum at the stable fixed point a_1 and is not bounded from below. In the limit that $\Delta \to \infty$, $E[a_3] \to E[a_1]$ and the amplitudes of the corresponding fixed points also approach another, as is clear from fig. 8.

For energy values in the range $E[a_2] \leq E \leq E[a_3]$, there is a two-fold degeneracy of curves. This occurs because as we proceed towards negative u from the unstable fixed point (at amplitude a_3), the energy decreases without bound from the value $E[a_3]$ while if we proceed towards positive u

from this point, the energy again decreases to a minimum of $E[a_2]$ and then increases to a maximum of $E[a_1]$ at the stable fixed point at a_1. One set of curves in the above range are the relatively small amplitude motions about the stable fixed point $(a_2, 0)$ and contained within the homoclinic loop. On these contours, $R^2 = R_-^2$. In the same range of energies, there is another set of curves with larger amplitudes lying outside the homoclinic loop. If these curves are completely outside the circle of radius $\sqrt{\Delta/\lambda}$, then $R^2 = R_+^2$ on the complete contour, otherwise $R^2 = R_-^2$ on the portion of the contour lying within the circle. Figure 12 shows the equal energy contours for a few values of E at $\Delta = 2.00$, at a detuning above the bifurcation value of $\Delta_{bf} = 0.859$.

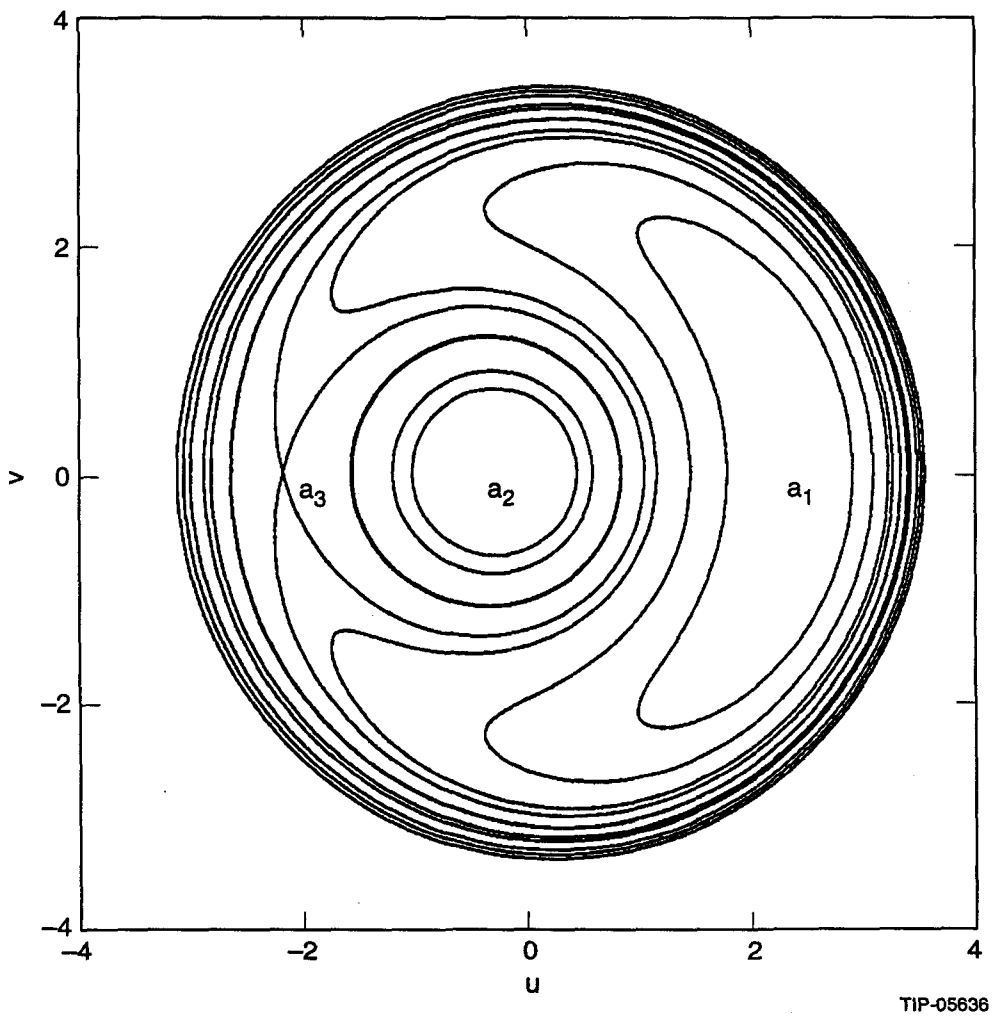

Fig. 12. Equal energy contours in (u, v) phase space for a detuning above the bifurcation value; $\lambda = 3/8$, $\kappa = 0.5$, $\Delta = 2.0$. The fixed points are at $(u_{c1}, v_{c1}) = (2.425, 0.0)$, $(u_{c2}, v_{c2}) = (-0.253, 0.0)$ and $(u_{c3}, v_{c3}) = (-2.172, 0.0)$.

4.4. Solution of the averaged equations

In this section we show that the solution of the averaged equations (4.25), (4.26) can be written in terms of Jacobian elliptic functions. These exact solutions will be used later in calculating the time evolution and also the long time limit of ensemble averages. If we let

$$u = \sqrt{2J}\cos\gamma \quad \text{and} \quad v = \sqrt{2J}\sin\gamma \tag{4.34}$$

then (J, γ) are canonically conjugate variables whose equations of motion are

$$\gamma' = \Delta - 2\lambda J + \frac{\kappa}{\sqrt{2J}}\cos\gamma \tag{4.35}$$

$$J' = \kappa\sqrt{2J}\sin\gamma \ . \tag{4.36}$$

These are derivable from the Hamiltonian

$$H = -\lambda J^2 + \Delta J + \kappa\sqrt{2J}\cos\gamma \tag{4.37}$$

with

$$\gamma' = \frac{\partial H}{\partial J} \ , \quad J' = -\frac{\partial H}{\partial \gamma} \ . \tag{4.38}$$

The fact that H is independent of the time (η) implies that the equations are integrable by quadrature. We can eliminate γ from the equations of motion and integrate the resulting equation for J to obtain

$$\int_{J_0}^{J} \frac{dJ'}{\sqrt{2\kappa^2 J' - (E + \lambda J'^2 - \Delta J')^2}} = \mathrm{sgn}(\sin\gamma_0)\int_{\eta_0}^{\eta} d\eta \ . \tag{4.39}$$

We represent the constant value of the Hamiltonian by the energy E. γ_0 is the initial value of γ and the prefactor $\mathrm{sgn}(\sin\gamma_0)$ is the sign of $\sin\gamma_0$. This factor indicates whether J is increasing or decreasing at the initial instant. For a given energy, the excursions in J are bounded between a lower and an upper limit, J_{min} and J_{max} respectively. At these limits, the denominator in the left hand side of the above equation vanishes. The quartic expression in this denominator can be factored either as

$$2\kappa^2 J - (E + \lambda J^2 - \Delta J)^2 = \lambda^2 (J_{max} - J)(J - J_c)(J - J_c^*)(J - J_{min}) \tag{4.40}$$

where J_c, J_c^* are complex conjugate roots or as

$$2\kappa^2 J - (E + \lambda J^2 - \Delta J)^2 = \lambda^2 (J_{max} - J)(J - J_{low})(J - J_{high})(J - J_{min}) \tag{4.41}$$

where all roots are real and $J_{min} < J_{max}$, $J_{low} < J_{high}$. We consider the two cases separately.

(a) Two real and two complex roots

There are only two real roots at all energies if $\Delta < \Delta_{bf}$ while for $\Delta > \Delta_{bf}$ this is true if either $E < E[a_2]$ or if $E > E[a_3]$. We change the variable of integration from J to a variable y defined over the entire positive real axis,

$$y = \sqrt{\frac{J - J_{min}}{J_{max} - J}}, \qquad 0 \leq y \leq \infty \ .$$

We also define the complex parameters α, ΔJ and real parameter y_0 as

$$\alpha = \frac{J_{min} - J_c}{J_{max} - J_c}, \ |\alpha| \leq 1 \quad ; \quad y_0 = \sqrt{\frac{J_0 - J_{min}}{J_{max} - J_0}} \quad ; \quad \Delta J = J_{max} - J_c \ .$$

Then Eq. (4.39) can be written as

$$\int_{y_0}^{y} \frac{dy'}{\sqrt{(y'^2 + \alpha)(y'^2 + \alpha^*)}} = \mathrm{sgn}(\sin\gamma_0)\frac{\lambda|\Delta J|}{2}(\eta - \eta_0) \ . \tag{4.42}$$

We can use the time translation invariance of the equations of motion to set the initial instant η_0 to be zero without loss of generality. Using the table of integrals in [15], we obtain after integrating the above equation,

$$\frac{1}{2\sqrt{|\alpha|}}\Big[F(\phi_0, k) - F(\phi, k)\Big] = \frac{\lambda|\Delta J|}{2}\eta \ . \tag{4.43}$$

$F(\phi, k)$ is the incomplete elliptic function of the first kind. The real parameters k, ϕ_0 and the variable ϕ are defined as follows

$$k = \frac{1}{\sqrt{2}}\sqrt{1 - \frac{\mathrm{Re}(\alpha)}{|\alpha|}} \ , \ \phi_0 = \mathrm{arcos}\left(\frac{y_0^2 - |\alpha|}{y_0^2 + |\alpha|}\right) \ , \ \phi = \mathrm{arcos}\left(\frac{y^2 - |\alpha|}{y^2 + |\alpha|}\right) \ .$$

The solution for y can be transformed back into a solution for the amplitude squared variable J. Defining the time dependent parameter χ as

$$\chi = F(\phi_0, k) - \mathrm{sgn}(\sin\gamma_0)\lambda\sqrt{|J_{max} - J_c||J_{min} - J_c|}\eta \tag{4.44}$$

the solution for J is

$$J = \frac{|\alpha|J_{max} + J_{min} + (|\alpha|J_{max} - J_{min})\mathrm{cn}\chi}{1 + |\alpha| - (1 - |\alpha|)\mathrm{cn}\chi} \tag{4.45}$$

where $\mathrm{cn}(\chi, k)$, the Jacobean elliptic cosine function, is a doubly periodic function with a real period of $4K(k)$, $K(k)$ being the complete elliptic function of the first kind. This shows that J is a periodic function of η. Equation (4.45) shows that J is a constant whenever $J_{min} = J_{max}$ (which implies $\alpha = 1$). This is true both at the stable fixed points and at the other limit, far away from the fixed points, where the motion is a simple harmonic oscillation. In the intermediate region of phase space, J varies significantly with time.

The phase space variables (u, v) can be obtained from J as

$$u = \frac{1}{\kappa}[E + \lambda J^2 - \Delta J] \quad , \quad v = \pm\sqrt{2J - u^2} \ . \tag{4.46}$$

The fundamental frequency Ω of motion on a curve is a function of the energy E on the curve, the turning points J_{min} and J_{max} are determined by the energy at constant λ, Δ, κ. From Eq. (4.44) we obtain,

$$\Omega(E) = \frac{\pi\lambda\sqrt{|J_{max} - J_c||J_{min} - J_c|}}{2K(k)} \ . \tag{4.47}$$

(b) Four real roots

The quartic expression may have four real roots if the detuning parameter Δ is above the bifurcation value Δ_{bf}. The motion is bounded between J_{min} and J_{max} with the other real roots of the quartic being J_{low} and J_{high}. This occurs if the energy lies in the range $E[a_2] \leq E \leq E[a_3]$ where $E[a_2]$ is the energy at the stable fixed point $(u_{c2}, v_{c2}) = (-a_2, 0)$ and $E[a_3]$ is the energy at the unstable fixed point $(u_{c3}, v_{c3}) = (-a_3, 0)$. The integral is

$$\int_{J_0}^{J} \frac{dJ}{\sqrt{(J_{max} - J)(J - J_{min})(J - J_{high})(J - J_{low})}} = \mathrm{sgn}(\sin\gamma_0)\lambda\eta$$

with the two possibilities for the ordering of the roots $J_{max} > J_{min} > J_{high} > J_{low}$ or $J_{high} > J_{low} > J_{max} > J_{min}$. There are two curves with the same energy, the first ordering holds for the large amplitude curve and the second ordering applies to the smaller amplitude curve which is enclosed within the inner homoclinic loop. The above integral can be evaluated using the table of integrals in [15]. Define the parameters:

$$a = \frac{J_{max} - J_{min}}{J_{high} - J_{min}} \ , \qquad \phi_0 = \arccos\left(\sqrt{\frac{(J_{high} - J_{min})(J_{max} - J_0)}{(J_{max} - J_{min})(J_{high} - J_0)}}\right) \ ,$$

$$k = \sqrt{\frac{(J_{high} - J_{low})(J_{max} - J_{min})}{(J_{high} - J_{max})(J_{low} - J_{min})}} \ .$$

The corresponding time dependent parameter is defined as

$$\chi = F(\phi_0, k) + \frac{1}{2}\mathrm{sgn}(\sin\gamma_0)\lambda\sqrt{(J_{high} - J_{max})(J_{low} - J_{min})}\ \eta \ .$$

The solution for J is

$$J = \frac{J_{max} - J_{high}\ a\ \mathrm{cn}^2\chi}{1 - a\ \mathrm{cn}^2\chi} \ . \tag{4.48}$$

The degenerate case that two of the four real roots are equal corresponds to particle motion on the homoclinic orbit.

The corresponding energy dependent frequency is

$$\Omega(E) = \frac{\pi\lambda\sqrt{(J_{high} - J_{max})(J_{low} - J_{min})}}{4K(k)} . \tag{4.49}$$

Note that $\Omega(E)$ is invariant under the interchange $J_{min} \leftrightarrow J_{low}$, $J_{max} \leftrightarrow J_{high}$. This proves the somewhat surprising result that the frequency of motion on both the small amplitude curve and the large amplitude curve of equal energy is the same.

4.5. Fundamental frequency and Fourier coefficients of the solution

We know that each solution (u, v) is periodic in the slow time variable η with fundamental frequency $\Omega(E)$, and hence can be expanded as a Fourier series in $\Omega(E)$. The dependence of Ω on the energy is different in the two cases $\Delta < \Delta_{bf}$ and $\Delta > \Delta_{bf}$. Figures 13 and 14 show how the frequency varies with energy at three values of the detuning below and above the bifurcation value Δ_{bf}, respectively.

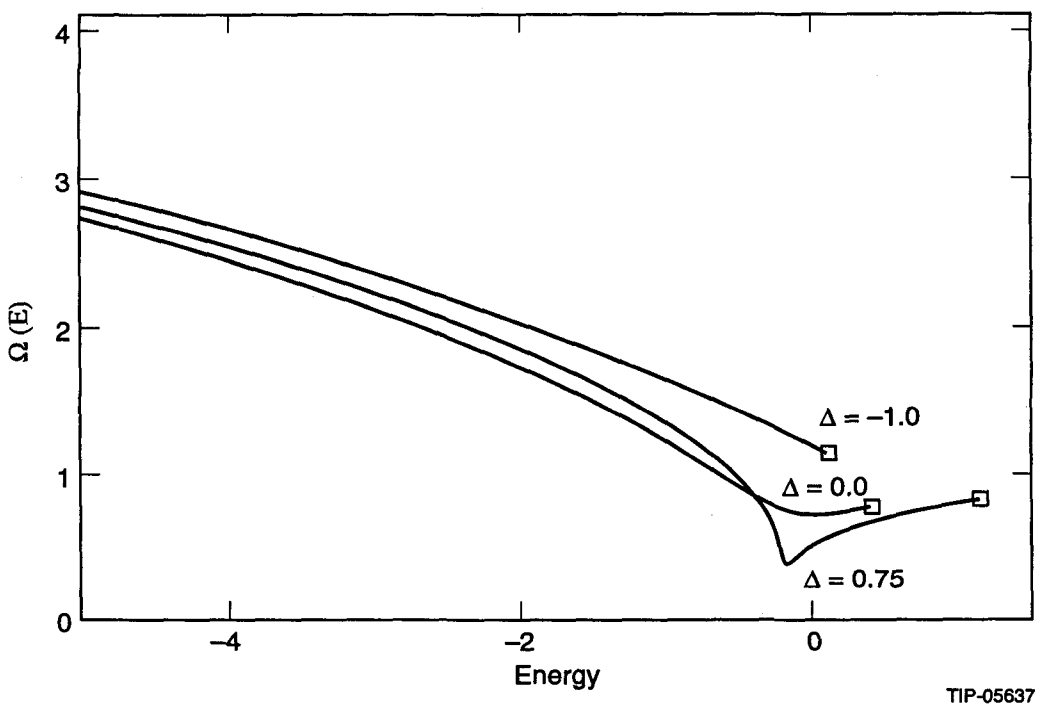

Fig. 13. Frequencies $\Omega(E)$ below the bifurcation value of the detuning; $\lambda = 3/8$, $\kappa = 0.5$. □ shows the location of the stable fixed point. The frequency shown in this plot is measured in units of the slow time $\epsilon\omega_r/\omega_0$.

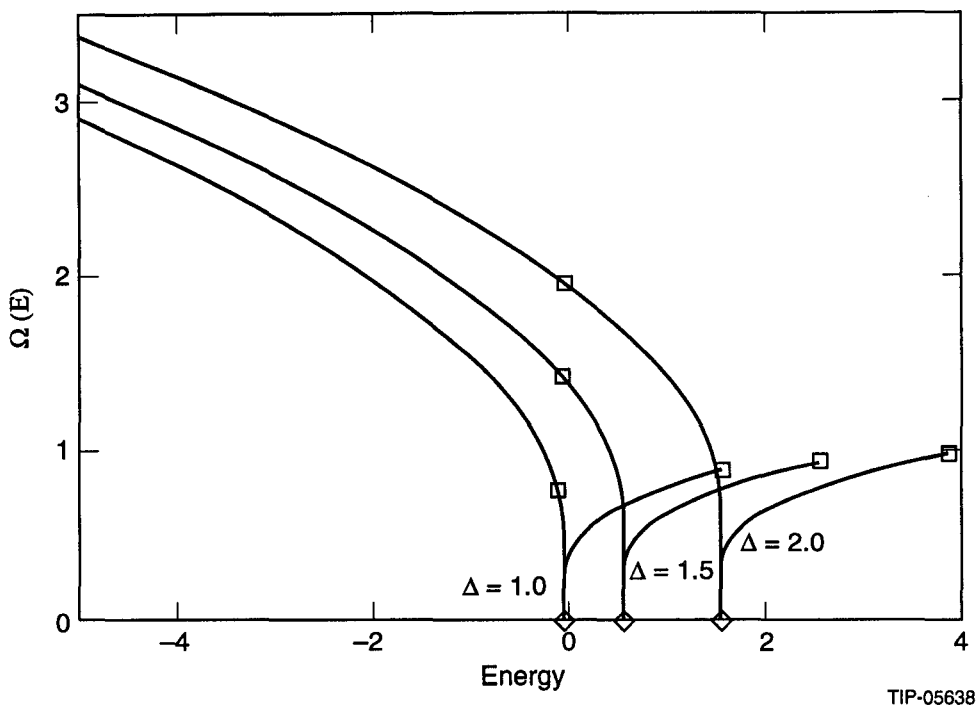

Fig. 14. Frequencies $\Omega(E)$ above the bifurcation value of the detuning; $\lambda = 3/8$, $\kappa = 0.5$. On each curve □ shows the locations of the two stable fixed points while ◇ shows the unstable fixed point.

For large negative values of Δ, the minimum frequency is at the fixed point and increases monotonically as the energy becomes more negative. As the detuning increases towards zero, the minimum of the frequency shifts away from the fixed point and also decreases in value. The minimum approaches zero and its depth increases as Δ increases and approaches the bifurcation value. For $\Delta > \Delta_{bf}$, the minimum is an asymmetric cusp at the energy corresponding to the homoclinic loop and the frequency vanishes. As proved in Section 4.4(b), $\Omega(E)$ is a single-valued function of energy over the entire range.

The fact that at large negative energies the frequency increases with energy can also be seen from the equations of motion for (u, v). From (4.25) and (4.26), we find that at large amplitudes, $R^2 = u^2 + v^2$ is essentially a constant of the motion and the frequency is $\Omega \approx \lambda R^2 \approx 2\sqrt{\lambda}\sqrt{-E}$.

To expand J in a Fourier series as,

$$J = \sum_{n=-\infty}^{n=\infty} \tilde{J}_n e^{in\Omega(E)[\eta-\eta_0]} \tag{4.50}$$

we use the Fourier expansion of the cn function [15],

$$\mathrm{cn}(\chi, k) = 2\sum_{n=0}^{\infty} c_n \cos(2n+1)\nu$$

where the parameters are defined as

$$\nu = \frac{\pi}{2K(k)}\chi = \frac{\pi F(\phi_0, k)}{2K(k)} - \mathrm{sgn}(\sin\gamma_0)\Omega(E)\eta$$

$$q = \exp\left(-\pi\frac{K'(k)}{K(k)}\right) \ , \ K'(k) = K(\sqrt{1-k^2}) \ .$$

and the coefficients are

$$c_j = \frac{\pi}{kK(k)}\frac{q^{j/2}}{1+q^j} \ , \qquad j = 1, 3, \ldots$$

$$= 0 \ , \qquad j = 0, 2, 4, \ldots$$

The function J being real requires that the complex coefficients $\tilde{J}_n$ obey $\tilde{J}_{-n} = \tilde{J}_n^*$. From the numerical computations of Section 3 it is clear that in the range of external forces considered here, only the first few harmonics in $\Omega(E)$ are important. Accordingly we drop all coefficients $\tilde{J}_n$ for n greater than 3. This will be justified a posteriori by the results. Here we will use the solution when there are two real roots. A similar procedure can be performed in the other case. Let

$$J_1 = |\alpha|J_{max} + J_{min}, \quad J_2 = |\alpha|J_{max} - J_{min}, \quad J_3 = 1 + |\alpha|, \quad J_4 = -\Big(1 - |\alpha|\Big) \ .$$

We substitute the Fourier expansions of J and the cn function into the following equation (obtained from Eq. (4.45)),

$$J\Big[1 + |\alpha| - \Big(1 - |\alpha|\Big)\mathrm{cn}\chi\Big] = |\alpha|J_{max} + J_{min} + \Big(|\alpha|J_{max} - J_{min}\Big)\mathrm{cn}\chi \ . \tag{4.51}$$

Solving the 4×4 set of linear equations for the coefficients $\tilde{J}_n$, we find that the imaginary parts of the coefficients vanish identically and the real parts are given by,

$$\tilde{J}_0 = \frac{1}{D}\Bigg(J_1J_3\Big[J_3^2 - J_4^2\Big[(c_1+c_3)^2 + (c_1+c_5)^2\Big]\Big]$$
$$+2J_2J_4\Big[J_4^2\Big[c_1(c_1+c_5) - c_3(c_1+c_3)\Big] - J_3^2(c_1^2+c_3^2)\Big]\Bigg) = \frac{1}{D}\Big[J_1J_3^3 + O(c_1^2)\Big]$$

$$\tilde{J}_1 = \frac{1}{D}(J_2J_3 - J_1J_4)\Big[J_3^2c_1 - J_4^2c_1(c_1+c_5)^2 + J_4^2c_3(c_1+c_3)(c_1+c_5)\Big]$$
$$= \frac{1}{D}(J_2J_3 - J_1J_4)\Big[J_3^2c_1 + O(c_1^3)\Big]$$

$$\tilde{J}_2 = -\frac{1}{D}(J_2J_3 - J_1J_4)J_3J_4[c_1^2 + 2c_1c_3 + c_3c_5]$$

$$= -\frac{1}{D}(J_2J_3 - J_1J_4)J_3J_4\Big[c_1^2 + O(c_1^4)\Big]$$

$$\tilde{J}_3 = \frac{1}{D}(J_2J_3 - J_1J_4)\Big[J_3^2c_3 + J_4^2(c_1+c_3)\Big[c_1(c_1+c_5) - c_3(c_1+c_3)\Big]\Big]$$

$$= \frac{1}{D}(J_2J_3 - J_1J_4)\Big[J_4c_1^3 + J_3^2c_3 + O(c_1^5)\Big]$$

where D is the determinant of the 4×4 matrix,

$$D = J_3^4 - J_3^2J_4^2\Big[2(c_1^2+c_3^2) + (c_1+c_3)^2 + (c_1+c_5)^2\Big] + 2J_4^4\Big[c_1(c_1+c_5) - c_3(c_1+c_3)\Big]^2 \ .$$

These solutions show that the leading term in each coefficient $\tilde{J}_n$ is proportional to c_1^n or equivalently to $\exp[-n\pi K'(k)/K(k)]$. The prefactor of this coefficient (e.g. J_3^2 in $\tilde{J}_1$, J_3J_4 in $\tilde{J}_2$ etc.) also decreases with increasing n. This indicates that the Fourier coefficients $\tilde{J}_n$ are decreasing exponentially, barring the singular case for $k = 1$. This explains why only a few harmonics contribute significantly to the motion at the forcings we consider in this paper. The second point to be noticed is that since $J_2J_3 - J_1J_4 = 2|\alpha|(J_{max} - J_{min})$, the three coefficients $\tilde{J}_n$, $n > 0$ are proportional to $J_{max} - J_{min}$. We know that when $J_{max} = J_{min}$ only the coefficient $\tilde{J}_0$ will be non-zero. Hence we can expect that $\tilde{J}_n$ is proportional to $J_{max} - J_{min}$ for all $n > 0$.

Since the Fourier expansion of J contains only a small number (say N_J) of significant coefficients, it follows from

$$u = \frac{1}{\kappa}[E + \lambda J^2 - \Delta J]$$

that u has at most $2N_J$ significant Fourier coefficients. If we keep coefficients to the same order as we did for J, we retain only N_J of these coefficients. The Fourier expansion for v is most conveniently obtained from the equation of motion

$$v' = \kappa - (2\lambda J - \Delta)u \ .$$

Since v is a periodic function,v' is a periodic function with zero mean and we are justified in dropping the constant terms on the right hand side of the above equation. Integrating, we obtain a Fourier expansion for v and retain only the N_J most significant coefficients. Thus we can write

$$\begin{aligned} u &= \tilde{u}_0 + \tilde{u}_1\cos\nu + \tilde{u}_2\cos 2\nu + \dots \\ v &= \tilde{v}_0 + \tilde{v}_{1C}\cos\nu + \tilde{v}_{1S}\sin\nu + \tilde{v}_{2C}\cos 2\nu + \tilde{v}_{2S}\sin 2\nu + \dots \end{aligned} \tag{4.52}$$

Substituting this back into the expression for x,

$$x = u\cos\omega_r t + v\sin\omega_r t + O(\epsilon) \tag{4.53}$$

we see that x (and also $\dot{x}$) are quasi-periodic functions of t with two base frequencies. Writing out the first few terms in the expansion for x, we obtain

$$x = \tilde{u}_0 \cos\omega_r t + \tilde{v}_0 \sin\omega_r t + \frac{1}{2}\Big[(\tilde{u}_1 - \tilde{v}_{1S})\cos(\omega_r t + \nu) + \tilde{v}_{1C}\sin(\omega_r t + \nu)\Big]$$

$$+\frac{1}{2}\Big[(\tilde{u}_1 + \tilde{v}_{1S})\cos(\omega_r t - \nu) + \tilde{v}_{1C}\sin(\omega_r t - \nu)\Big] + \ldots \tag{4.54}$$

This shows that x has Fourier components at frequencies ω_r, $\omega_r \pm \epsilon\Omega(E)$, $\omega_r \pm 2\epsilon\Omega(E), \ldots$ The first few of these are seen in figs. 2, 3 and 4.

In Section 2 for the collection of linear oscillators, a similar solution was used to calculate the ensemble average by averaging over the initial conditions. In principle, the above perturbative solution could be also be similarly used to calculate the ensemble average. In practice this is hard to do analytically because the coefficients $(\tilde{u}_j, \tilde{v}_{jC}, \tilde{v}_{jS})$ and ν depend on the initial conditions in a complicated way. Instead we must use the equilibrium phase space density to calculate the long time averages.

In fig. 15 we see how the dominant frequency in x changes with the average amplitude of the particle at a detuning where there is only one fixed point. We see that all particles which respond at the drive frequency $\omega_r (= 0.99$ in the figure) have amplitudes close to the fixed point while particles which are driven to average amplitudes larger than the fixed point amplitude respond at the amplitude dependent larger frequency $\omega_r + \epsilon\Omega(E)$. The gap in the frequency spectrum between ω_r and the next value of the response frequency occurs because here the minimum value of $\Omega(E)$ is positive.

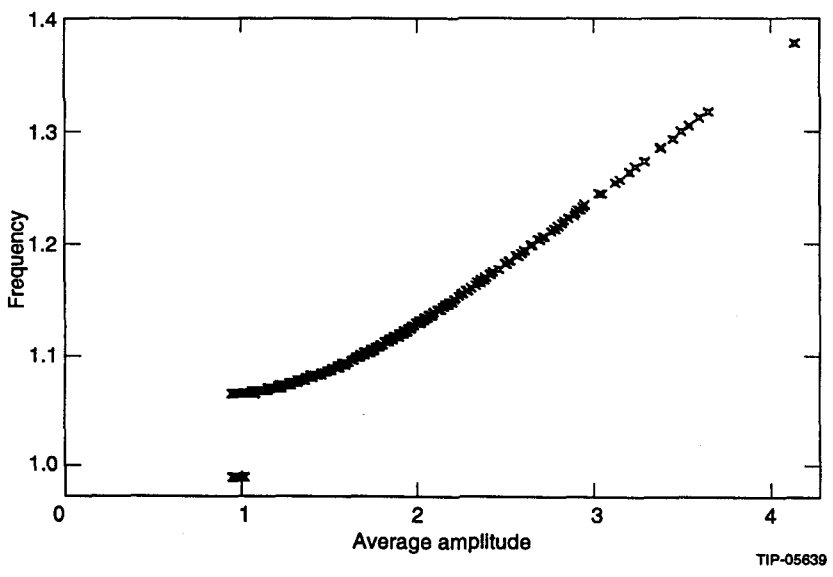

Fig. 15. Dominant frequency in $x(t)$ for 1000 particles as a function of the average amplitude. The frequency is obtained by an FFT of the numerically integrated Duffing equation. Parameters: $\epsilon = 0.1$, $f = 1.0$, $\Delta = -0.1$. The driving frequency is $\omega_r = 0.99$.

5. Collective behavior and the long time limit

For linear oscillators, the ensemble averages of any dynamical quantity can be calculated by averaging the exact solutions over the initial conditions. The behavior at long times can be obtained by finding the long time asymptotics of the ensemble average, as was done in Section 2. For a collection of non-linear oscillators we cannot do this for two reasons. In general solutions in terms of known functions do not exist and secondly even a perturbative solution has a complicated dependence on the initial conditions which precludes such an averaging procedure. Instead we must turn to a statistical description of the ensemble behavior.

The differential equation governing the evolution of the forced oscillator is

$$\frac{d\mathbf{x}}{d\tau} = J\mathbf{x} + \epsilon\mathbf{g}(\mathbf{x},\tau) + \epsilon^2\mathbf{h} \tag{5.1}$$

with initial conditions $\mathbf{x}(\tau_0) = \mathbf{x}_0$. Given an initial density $p_0(\mathbf{x})$, our goal is to understand the evolution of the phase space density $p(\mathbf{x},\tau)$. From the divergence-less nature of the vector field governing the flow of $\mathbf{x}$, it follows that (see Appendix B),

$$p(\mathbf{x},\tau) = p_0\Big(\vec{\Psi}(\tau_0,\tau,\mathbf{x})\Big) \tag{5.2}$$

where $\mathbf{x}(\tau) = \vec{\Psi}(\tau,\tau_0,\mathbf{x}_0)$ is the general solution of the initial value problem (5.1). From our discussion in Section 4.1 we have

$$\mathbf{x}(\tau) = e^{\mathbf{J}(\tau-\tau_0)}\mathbf{y}(\tau)$$

and

$$\mathbf{y} = \mathbf{u} + \epsilon\mathbf{P}(\mathbf{u},\tau,\tau_0) + O\Big(\epsilon^2(\tau-\tau_0)\Big)$$

where $\mathbf{u}$ is defined by

$$\frac{d\mathbf{u}}{d\tau} = \epsilon\bar{\mathbf{G}}(\mathbf{u},\tau_0) \tag{5.3}$$

with initial conditions $\mathbf{u}(\tau_0) = \mathbf{x}_0$. The general solution of (5.3) will be denoted $\mathbf{u}(\tau) = \vec{\phi}(\tau,\tau_0,\mathbf{x}_0)$. As previously discussed, (5.3) is an autonomous (Hamiltonian) system in the plane and all solutions are periodic, except for the homoclinic loop in the case that there are three fixed points. Liouville's theorem then assures us that phase volumes are conserved in the time evolution and specifically that the phase space density at time τ may be obtained by evolving the particle trajectories backwards in time by an amount τ as discussed in Appendix B. Since the solutions of the averaged equations are periodic, the phase space density in $\mathbf{u}$ space, $\rho(\mathbf{u},\tau) = \rho_0(\vec{\phi}(\tau_0,\tau,\mathbf{u})) = p_0(\vec{\phi}(\tau_0,\tau,\mathbf{u}))$, is a periodic function of τ and does not have a long time limit. The periods $T(E)$ on the phase space curves

depend non-trivially upon the energy E and thus we expect that there exists an equilibrium density $\rho_{eq}(H(\mathbf{u}))$ such that a long time limit exists in the following coarse-grained sense,

$$\lim_{\tau\to\infty}\int_A \rho(\mathbf{u},\tau)\,d\mathbf{u} = \int_A \rho_{eq}\Big(H(\mathbf{u})\Big)d\mathbf{u} \tag{5.4}$$

for all sufficiently well behaved regions A. A proof of this assertion (for a special class of A) in the problem of particle channeling in crystals can be found in [16] and we believe that the proof can be generalized to cover the case of this paper although some care is clearly needed near the homoclinic loop. A crucial point in the proof is that the period $T(E)$ must have a non-zero derivative except at isolated points. For a collection of non-interacting linear oscillators with the same frequency, the density is also a periodic function of time. However all phase curves have the same period and consequently no limit exists, even in the sense of (5.4).

By the averaging theorem

$$\mathbf{x}(\tau_0+2n\pi) = \mathbf{y}(\tau_0+2n\pi) = \mathbf{u}(\tau_0+2n\pi) + O(\epsilon)$$

for integer $n = O(1/\epsilon)$. In addition, we expect the flow in $\mathbf{u}$ space to equilibrate in a duration τ of $O(1/\epsilon)$ and if this is the case, then

$$p(\mathbf{x},\tau_0+2n\pi) = p_0\Big(\vec{\Psi}(\tau_0,\tau_0+2n\pi,\mathbf{x})\Big) = p_0\Big(\vec{\phi}(\tau_0,\tau_0+2n\pi,\mathbf{x})\Big) + O(\epsilon) \tag{5.5}$$

should have a coarse grained limit, i.e

$$\lim_{n\to\infty}\int_A p(\mathbf{x},\tau_0+n)\,d\mathbf{x} = \int_A \rho_{eq}\Big(H(\mathbf{u})\Big)d\mathbf{u} + O(\epsilon)\ . \tag{5.6}$$

While this may seem somewhat optimistic, recall that the adiabatic invariance result of [13] does give that $\mathbf{x}(\tau_0+2\pi n)$ follows the integral curves of the averaged motions quite accurately until $n = O(1/\epsilon^2)$. Furthermore, our numerical calculations also give evidence for equilibration. In this paper we do not examine (5.6) itself because we are interested in specific ensemble averages defined by

$$\langle f(\mathbf{x})\rangle(\tau) = \int_{\text{all } \mathbf{x}} f(\mathbf{x})p(\mathbf{x},\tau)\,d\mathbf{x}\ . \tag{5.7}$$

From (5.6) and the averaging and adiabatic invariant results we are optimistic that on a surface of section,

$$\begin{aligned}\lim_{n\to\infty}\Big\langle f(\mathbf{x})\Big\rangle(\tau_0+2n\pi) &= \lim_{n\to\infty}\Big\langle f(\mathbf{u})\Big\rangle(\tau_0+2n\pi) + O(\epsilon)\\ &\to \Big\langle f(\mathbf{u})\Big\rangle_{eq} + O(\epsilon)\ .\end{aligned} \tag{5.8}$$

In Section 8 we present numerical evidence for this.

The equilibrium density ρ_{eq} is obtained by distributing the initial density p_0 uniformly on thin energy shells in $\mathbf{u}$ phase space. In the following section we discuss the construction of ρ_{eq} and the approach to the above limit.

As a point of interest we note that the averaged equations of motion (4.25) and (4.26) possess a scale invariance which can be used to reduce the number of independent parameters both in the equations of motion and in the ensemble averages. The variables (u, v) and the time η can be scaled as

$$u = \beta U \ , \ v = \beta V \ , \ \eta = \frac{1}{\Delta}\tilde{\eta}$$

where $\beta = \sqrt{\Delta/\lambda}$ such that the equations of motion depend on only one parameter $K = \kappa\sqrt{\lambda/\Delta^3}$,

$$\frac{dU}{d\tilde{\eta}} = -V + V(U^2 + V^2) \tag{5.9}$$

$$\frac{dV}{d\tilde{\eta}} = K + U - V(U^2 + V^2) \ . \tag{5.10}$$

The scaled energy $\mathcal{E}$ is related to the original energy E by $\mathcal{E} = \lambda E/\Delta^2$. If $\psi_{eq}(\mathcal{E})$ be the equilibrium density distribution for the (U, V) variables, then it will depend on K through the equations of motion and on β though the initial conditions.

$$\psi_{eq}(\mathcal{E}, \beta, K) = \frac{\beta^2}{\Delta\mathcal{A}} \int\int_{\mathcal{E} \leq \mathcal{H}(U,V,K) \leq \mathcal{E}+\Delta\mathcal{E}} \rho_0(\beta U, \beta V) \ dU \ dV \ .$$

Thus for example the equilibrium value of $(u^2 + v^2)$ is given by

$$\langle u^2 + v^2 \rangle = \beta^2 \langle U^2 + V^2 \rangle \equiv \int\int \psi_{eq}(\mathcal{E}, \beta, K)(U^2 + V^2) \ dU \ dV \ .$$

Hence $\langle u^2 + v^2 \rangle$ depends on the parameters λ, Δ, κ through β and K, i.e,

$$\langle u^2 + v^2 \rangle = \langle u^2 + v^2 \rangle(\beta, K) \ .$$

Now β and K are invariant under the scaling transformations

$$\lambda \to c\lambda \ , \ \Delta \to c\Delta \ , \ \kappa \to c\kappa$$

where c is a constant. This implies that the ensemble averages are the same for parameter sets $(\lambda, \Delta, \kappa)$ related by the above transformation. However we do not make use of this property because in the accelerator problem, the nonlinearity parameter λ is fixed (it depends on the strength of the non-linear magnets) and is not a control variable.

6. Equilibrium density distribution

In the (u, v) plane, with the exception of motion on the homoclinic loop, particles move on closed curves symmetric about the u axis. These closed curves are labeled by the value of the Hamiltonian

H on the curve. The equilibrium density calculation assumes that an arbitrary initial distribution of points lying within a thin annulus $E \leq H \leq E + \Delta E$ will in time uniformize to an equilibrium phase space density distribution $\rho_{eq}(H(u,v))$ within a thin energy shell of area ΔA.

Consider a simple closed curve labeled by its energy E, and let S_E denote its interior and $A(E)$ be the area of S_E. By the conservation of particles,

$$\int\int_{S_{E+\Delta E}-S_E} \rho_{eq}\Big(H(u,v)\Big) du\, dv = \int\int_{S_{E+\Delta E}-S_E} \rho_0(u,v) du\, dv \tag{6.1}$$

where $\rho_0(u,v)$ is the initial density distribution. Expanding $\rho_{eq}\Big(H(u,v)\Big)$ around $H(u,v) = E$,

$$\rho_{eq}\Big(H(u,v)\Big) = \rho_{eq}(E) + O(\Delta E)$$

and making the canonical change of variables $(u,v) \rightarrow (E,\eta)$ via $(u,v) = \vec{\phi}(\eta, \mathbf{x}_0(E))$ where $\vec{\phi}(\eta, \mathbf{x}_0)$ is the general solution of (4.25) and (4.26) with $\vec{\phi}(0, \mathbf{x}_0) = \mathbf{x}_0$ and $\mathbf{x}_0(E)$ is chosen appropriately, gives

$$\rho_{eq}\Delta A + O(\Delta A \cdot \Delta E) = \int_E^{E+\Delta E} \int_0^{T(E')} \rho_0\Big(\vec{\phi}\Big(\eta, \mathbf{x}_0(E')\Big)\Big)\, d\eta\, dE' \ . \tag{6.2}$$

Dividing both sides by ΔE and taking the limit $\Delta E \rightarrow 0$, all but the first term on the left hand side vanish while the right hand side reduces to a single integral. Using the fact that

$$\frac{dA}{dE} = T(E) = \frac{2\pi}{\Omega(E)} \tag{6.3}$$

where $T(E)$ and $\Omega(E)$ are the period and frequency of motion on the curve with energy E, we obtain,

$$\rho_{eq}(E) = \frac{1}{T(E)} \int_0^{T(E)} \rho_0\Big(\vec{\phi}\Big(\eta, \mathbf{x}_0(E)\Big)\Big)\, d\eta \ . \tag{6.4}$$

This is the main result of this section: the equilibrium density on a closed curve of energy E is the time average of the initial density on this curve.

At a stable fixed point, $\vec{\phi}(\eta, \mathbf{x}_0(E_c)) = (u_c, v_c)$, where E_c denotes the energy at the fixed point, and therefore

$$\rho_{eq}(E_c) = \rho_0(u_c, v_c) \ , \tag{6.5}$$

i.e., the phase space density at the fixed point does not change with time. A complicated calculation given in Appendix C shows that

$$\rho'_{eq}(E_c) = \frac{\lambda u_c}{a^2 b}(3b + a) \frac{\partial \rho_0(u,v)}{\partial u}\bigg|_{(u_c,0)} - \frac{1}{2}\left(\frac{1}{a}\frac{\partial^2 \rho_0(u,v)}{\partial u^2}\bigg|_{(u_c,0)} + \frac{1}{b}\frac{\partial^2 \rho_0(u,v)}{\partial v^2}\bigg|_{(u_c,0)}\right) \ , \tag{6.6}$$

where $a = 3\lambda u_c^2 - \Delta$ and $b = \lambda u_c^2 - \Delta$.

It is important to keep in mind that $\rho_{eq}(H(u,v)=E)$ is the equilibrium phase space density. The energy density $\sigma(E)$ is given by

$$\sigma(E) = \rho_{eq}(E)\frac{dA}{dE} \tag{6.7}$$

and thus if E_{min} and E_{max} are the lower and upper limits of the energy in the given distribution of particles, then

$$2\pi \int_{E_{min}}^{E_{max}} \frac{\rho_{eq}(E)}{\Omega(E)}\, dE = 1 \ . \tag{6.8}$$

While the above expression (6.4) is conceptually simple, it requires the solution of the averaged equations in order to obtain the equilibrium density. This can be bypassed by taking u as the independent variable of integration, using the symmetry of the phase space curves about the u axis and writing $d\eta = -(\partial v/\partial E)\ du$, which follows from the equation of motion. Let $u_{min}(E)$ and $u_{max}(E)$ be the two turning points on the u axis, then

$$\rho_{eq}(E) = -\frac{\Omega(E)}{\pi}\int_{u_{min}(E)}^{u_{max}(E)} \frac{\partial v}{\partial E}(u,E)\ \rho_0\Big[u, v(u,E)\Big]\ du \ . \tag{6.9}$$

This expression is correct as written for phase portraits of the kind shown in fig. 10 where v is a single-valued function of u in all of phase space. However for portraits of the kind shown in figs. 11 and 12 where v is a double-valued function of u, the above integration must be modified to take into account the two segments on the curve. This will be done explicitly in the next section.

The symmetry of the phase space curves also simplifies the expression for the frequency $\Omega(E)$. Since the area $A(E)$ is given by

$$A(E) = \oint v\ du \tag{6.10}$$

it follows that the frequency is

$$\Omega(E) = \pi\left[\int_{u_{min}}^{u_{max}} \frac{\partial v}{\partial E}(u,E)\ du\right]^{-1} \ . \tag{6.11}$$

Given a distribution of particles, we can calculate the average over these particles of any dynamical variable at sufficiently long times such that the density has reached its equilibrium value. The average equilibrium value of $f(u,v)$ is given by

$$\Big\langle f(u,v)\Big\rangle_{eq} = \int_u\int_v f(u,v)\rho_{eq}\Big(H(u,v)\Big)du\ dv \ . \tag{6.12}$$

Using the variables (E,η) as before gives

$$\Big\langle f(u,v)\Big\rangle_{eq} = \int_{E_{min}}^{E_{max}} dE\rho_{eq}(E)\left[\int_0^{T(E)} f\Big(\phi_1\Big(\eta,\mathbf{x}_0(E)\Big),\phi_2\Big(\eta,\mathbf{x}_0(E)\Big)\Big)\ d\eta\right] \tag{6.13}$$

where all components at a given energy must be taken into account.

7. Calculation of the equilibrium density

Given an initial density distribution in $(x, \dot{x})$, we can calculate the equilibrium density distribution $\rho_{eq}(E)$ using the formulas derived in the previous section. We assume a Gaussian distribution centered about the origin, i.e.

$$p_0(x, \dot{x}) = \frac{1}{2\pi\sigma_x\sigma_{\dot{x}}} \exp\left[-\frac{1}{2}\left(\frac{x^2}{\sigma_x^2} + \frac{\dot{x}^2}{\sigma_{\dot{x}}^2}\right)\right] . \tag{7.1}$$

The Jacobian of the transformation from the $x(0), \dot{x}(0)$ variables to the initial variables in the (u, v) plane is

$$J\Big(x(0), \dot{x}(0) : u, v\Big) = \omega_r . \tag{7.2}$$

Using Eq. (6.9), we obtain for the equilibrium density

$$\rho_{eq}(E) = \frac{\Omega(E)\omega_r}{2\pi^2\sigma_x\sigma_{\dot{x}}} \int_{u_{min}}^{u_{max}} \frac{1}{(\lambda R^2 - \Delta)\sqrt{R^2 - u^2}} \exp\left[-\frac{1}{2}\left(\frac{u^2}{\sigma_x^2} + \frac{\omega_r^2[R^2 - u^2]}{\sigma_{\dot{x}}^2}\right)\right] du . \tag{7.3}$$

where R is a function of u given by Eq. (4.29). For negative values of Δ, the only singularity in the integrand is at the endpoints. However, for positive values of Δ, there is another singularity at $R^2 = \Delta/\lambda$ lying in the path of integration. This singularity occurs at a turning point u_{turn} for energies in the range $E_{low} \leq E \leq E_{high}$ given by Eq. (4.32). Hence for positive values of Δ, the integral for $\rho_{eq}(E)$ where E belongs in this range is evaluated as

$$\rho_{eq}(E) = \frac{\Omega(E)\omega_r}{2\pi^2\sigma_x\sigma_{\dot{x}}} \left\{ \int_{u_{turn}}^{u_{max}} \frac{1}{(\lambda R_+^2 - \Delta)\sqrt{R_+^2 - u^2}} \exp\left[-\frac{1}{2}\left(\frac{u^2}{\sigma_x^2} + \frac{\omega_r^2[R_+^2 - u^2]}{\sigma_{\dot{x}}^2}\right)\right] du \right.$$
$$\left. - \int_{u_{turn}}^{u_{min}} \frac{1}{(\lambda R_-^2 - \Delta)\sqrt{R_-^2 - u^2}} \exp\left[-\frac{1}{2}\left(\frac{u^2}{\sigma_x^2} + \frac{\omega_r^2[R_-^2 - u^2]}{\sigma_{\dot{x}}^2}\right)\right] du \right\} . \tag{7.4}$$

The integrals in the evaluation of the equilibrium density are evaluated numerically. The square-root singularities at the endpoints either in Eq. (7.3) or Eq. (7.4) can be treated using available codes [14]. It was noted in the previous section that the equilibrium density at the fixed point (u_c, v_c) equals the initial density at this point since all particles which are initially at this point stay there. Hence the equilibrium density at the maximum of the energy is

$$\rho_{eq}(E_{max}) = \frac{\omega_r}{2\pi\sigma_x\sigma_{\dot{x}}} \exp\left[-\frac{u_c^2}{2\sigma_x^2}\right] . \tag{7.5}$$

Figure 16 shows the equilibrium density as a function of energy at three values of the detuning below the bifurcation value $\Delta_{bf} = 0.859$ and the equilibrium phase space density is a smooth continuous function of the energy over the entire range $-\infty \leq E \leq E_{max} = E[a_0]$. Notice that the maximum stays near $E = 0$ which corresponds to the phase curve going through the origin where the

initial density ρ_0 is a maximum. The curves end at E_{max} corresponding to the stable equilibrium and the slope here is given by Eq. (6.6). This analytical expression for the slope can also be used to give a rough idea of our numerical accuracy, for example at $\kappa = 0.5, \Delta = -1.0$ the slope computed numerically is 0.06115 whereas the slope from (6.6) is 0.06114.

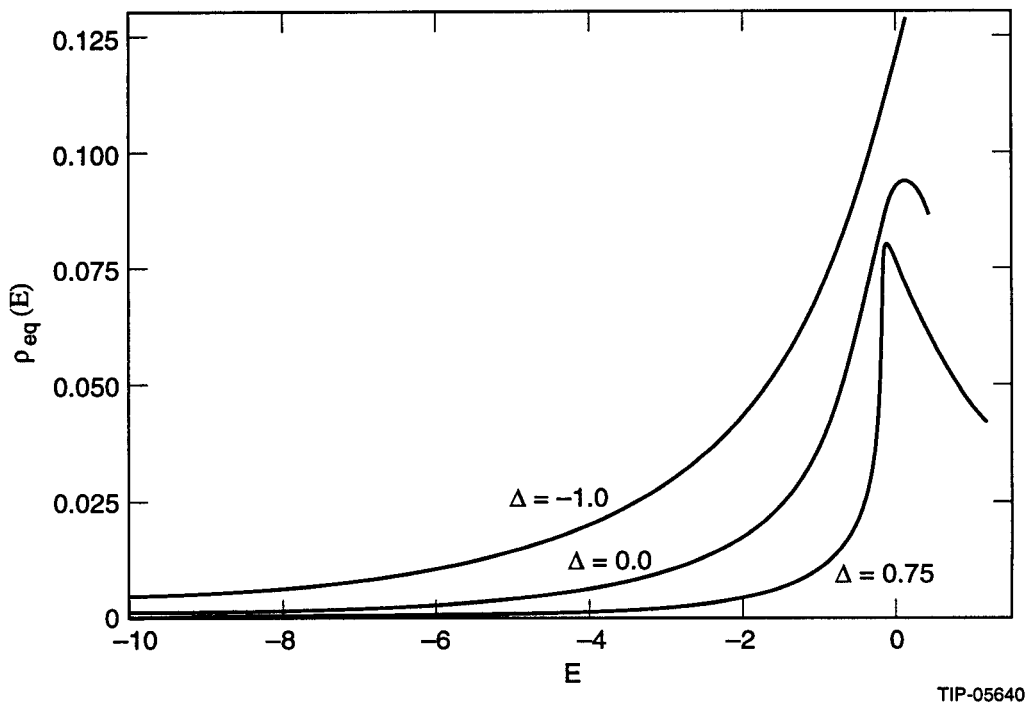

Fig. 16. Equilibrium phase space density $\rho_{eq}(E)$ at detunings Δ below the bifurcation value Δ_{bf}: $\lambda = 3/8$, $\kappa = 0.5$. The initial density is a Gaussian centered at the origin of phase space.

Figure 17 shows the density above the bifurcation value. Here the equilibrium phase space density $\rho_{eq}(E)$ has two branches and is double-valued in the range of energies $E[a_2] \leq E \leq E[a_3]$. The lower branch extends over the range $-\infty \leq E \leq E[a_3]$ while the upper branch extends over the range $E[a_2] \leq E \leq E[a_1]$. The double-valuedness occurs because there are two sets of curves with energies in this range, one set with small amplitude motions enclosed within the homoclinic loop and the other set with larger amplitudes outside the homoclinic loop (see fig. 12). The equilibrium density will be smaller in the region of phase space occupied by the second set of curves as can be seen in fig. 17.

We also note that $\rho_{eq}(E)$ has a jump discontinuity at $E = E[a_3]$, the energy on the homoclinic loop. The equilibrium density on the inner homoclinic loop is greater than the equilibrium density on the outer homoclinic loop. Hence the tip of the lower branch of $\rho_{eq}(E)$ does not touch the upper branch in the degenerate range $E[a_2] \leq E \leq E[a_3]$. The equilibrium density has a maximum at the stable fixed point $(u_{c2}, 0)$ to the left of the origin. A proof of this can be found in Appendix C. The

origin of this comes from two competing effects. The $E = 0$ phase curves contain the maximum initial density smeared out over the curve whereas the fixed point $(u_{c2}, 0)$ has a high density but no smearing.

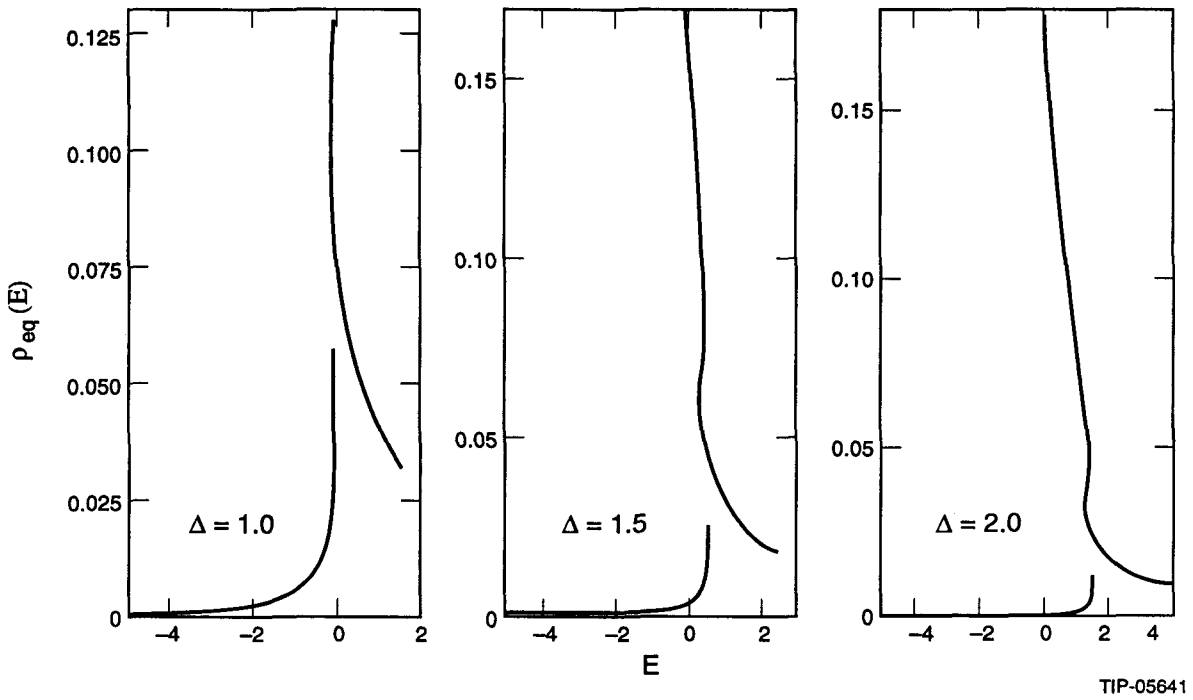

Fig. 17. Same as fig. 16 but at detunings Δ above the bifurcation value Δ_{bf}: $\lambda = 3/8$, $\kappa = 0.5$.

An alternative visualization of the variation of the equilibrium density $\rho_{eq}(E)$ along the phase space contours can be obtained by plotting these quantities as a function of the lower turning point u_{min} on the u axis. These are shown in figs. 18 and 19 for two values of Δ.

Figure 18 shows that for Δ below the bifurcation value Δ_{bf}, ρ_{eq} is a smooth continuous function of u_{min} with zero slopes at the fixed point and at another value of u_{min} where the maximum occurs. For Δ sufficiently negative, the maximum of ρ_{eq} is at the fixed point which is the only point of zero slope. This is because $a_0 \to 0$ for Δ sufficiently negative. Above the bifurcation value, u_{min} itself has a jump from $-a_2$ to the value where the homoclinic loop crosses the u axis between the two stable fixed points. This gap also shows up in the plot of ρ_{eq} in fig. 19. Also there is a discontinuity in ρ_{eq} at the unstable fixed point $-a_3$ because of the different densities on the two branches of the homoclinic loop.

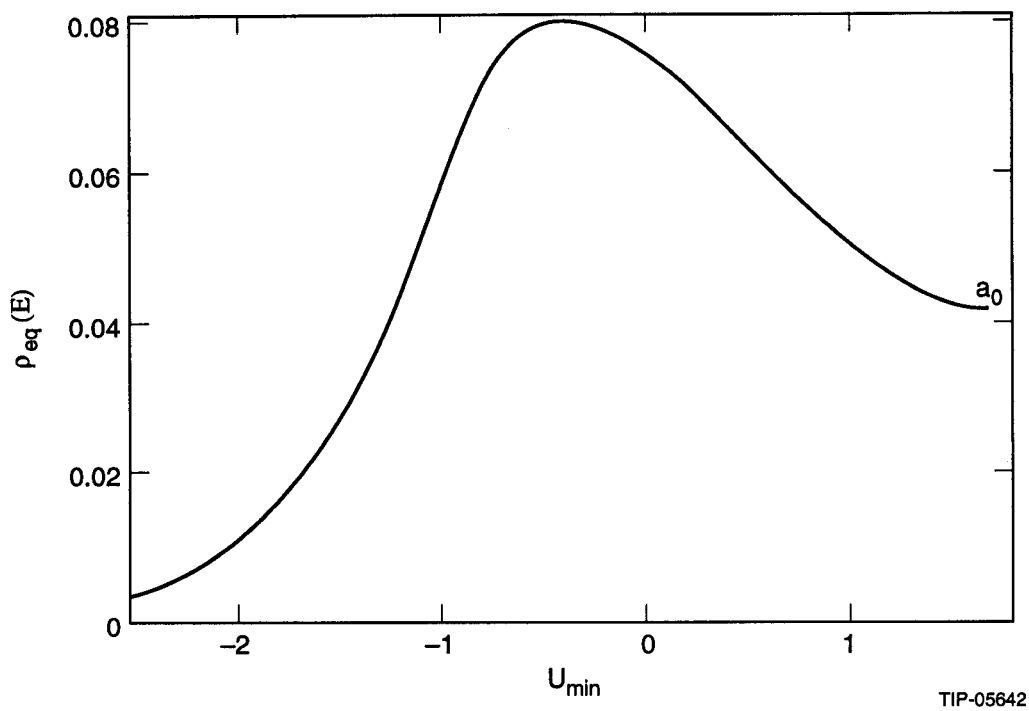

Fig. 18. Phase space equilibrium density as a function of u_{min} at a detuning Δ below the bifurcation value Δ_{bf}: $\lambda = 3/8$, $\kappa = 0.5$, $\Delta = 0.75$. The stable fixed point is at a_0.

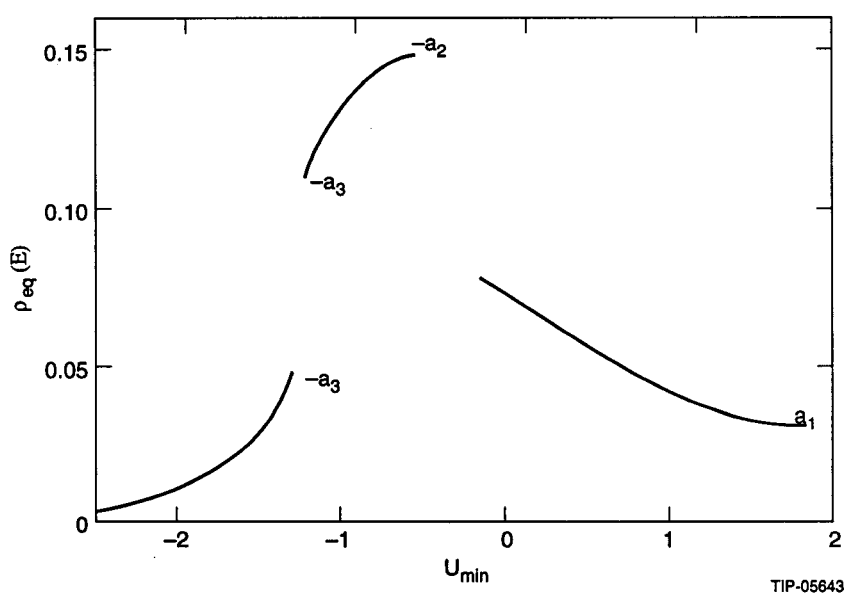

Fig. 19. Same as fig. 18 except at a detuning above the bifurcation value: $\lambda = 3/8$, $\kappa = 0.5$, $\Delta = 1.00$. The stable fixed points are at a_1 and $-a_2$ and the unstable fixed point is at $-a_3$. Refer to the text for an explanation of the discontinuities.

8. Ensemble averages and the approach to equilibrium

With the aid of the equilibrium phase space density, we can calculate the long time ensemble averages of any phase space variable. Two quantities that characterize the distribution of particles are the location of the centroid $\langle u\rangle_{eq}$ in physical space and the average amplitude squared $\langle R^2\rangle_{eq} = \langle u^2+v^2\rangle_{eq}$ in phase space. From the structure of the (u,v) equations, it is natural to consider u^2+v^2 and this explains our seemingly unnatural definition in Eq. (3.3). In relation to the accelerator problem, $\langle u\rangle_{eq}$ measures the transverse deviation of the beam from the central orbit and the change in $\langle R^2\rangle_{eq}$ is related to the growth of the emittance.

From Eq. (6.13), the ensemble average is

$$\Big\langle f(u,v)\Big\rangle_{eq} = \int_{E_{min}}^{E_{max}} T(E)\rho_{eq}(E) < f >_\eta (E)\, dE \equiv \int_{E_{min}}^{E_{max}} \sigma(E) < f >_\eta (E)\, dE \tag{8.1}$$

where $< f >_\eta (E)$ is the time average of f over a curve labeled by energy E, $T(E)$ is the period on this curve and $\sigma(E)$ is the equilibrium energy density. Specifically, the time average of R^2 is

$$< R^2 >_\eta (E) = \frac{1}{T(E)} \oint R^2 d\eta = \frac{\Omega(E)}{2\pi} \oint \frac{R^2}{u'} du = \frac{\Delta}{\lambda} + \frac{\Omega(E)}{\pi\lambda} \int_{u_{min}}^{u_{max}} \frac{du}{\sqrt{R^2-u^2}} \tag{8.2}$$

while the corresponding time average of u is

$$< u >_\eta (E) = \frac{\Omega(E)}{\pi} \int_{u_{min}}^{u_{max}} \frac{u}{(\lambda R^2-\Delta)\sqrt{R^2-u^2}}\, du\ . \tag{8.3}$$

Both these time averages can be calculated analytically in terms of the elliptic functions of the first, second and third kinds. However, since the time averages themselves of individual particles are not of interest here, we do not write them down. We note in passing that for particles at large energies, $< u >_\eta$ vanishes because the equations of motion (4.25) and (4.26) reduce to harmonic oscillator like equations at large amplitudes. Using the above expressions for the time averages, we obtain the equilibrium ensemble averages,

$$\langle R^2\rangle_{eq} = \frac{\Delta}{\lambda} + \frac{2}{\lambda} \int_{E_{min}}^{E_{max}} dE\ \rho_{eq}(E) \int_{u_{min}}^{u_{max}} \frac{du}{\sqrt{R^2-u^2}}$$

$$\langle u\rangle_{eq} = 2 \int_{E_{min}}^{E_{max}} dE\ \rho_{eq}(E) \int_{u_{min}}^{u_{max}} \frac{u}{(\lambda R^2-\Delta)\sqrt{R^2-u^2}}\, du\ . \tag{8.4}$$

We examine next the approach to the equilibrium value. We saw in Section 3 that the time for the ensemble average $\langle x^2+\dot{x}^2/\omega_r^2\rangle$ to relax to the equilibrium value depends strongly on the detuning, this time being at least an order of magnitude greater at $\Delta = -0.1$ than at $\Delta = 2.0$ for the same forcing amplitude. To understand the cause of this we study the relaxation to equilibrium of the ensemble average of u^2+v^2. The time evolution is calculated using the the exact solutions for u^2+v^2 obtained in Sections 4.4(a) and 4.4(b). The use of the exact solution prevents the

accumulation of round-off error at long times and the ensemble average can be calculated at any time without necessarily following the time evolution to that instant. For our calculation of the long time limit, we use 10^5 particles and evaluate the time average over 100 periods beginning at period 100,000. This number of particles is sufficiently large that the statistical error in averaging over a finite number of particles is smaller than the round-off error over 100 periods.

Figure 20 shows the evolution of $\langle R^2 \rangle$ at $\Delta = -0.1$, below the bifurcation value. The first maxima and the frequency of oscillations can be largely understood by assuming that the ensemble averages initially are dominated by particles where the density is large initially, i.e. near the origin where the energy $E = 0$. Over the first 88 periods there are 7 oscillations in $\langle R^2 \rangle$ leading to a period of 12.6 in units of the external drive period. A calculation of the time period using (4.47) shows that the time period of oscillations for $E = 0$ is $T(E) = 2\pi/0.77$ in units of the slow time $(\epsilon\omega_r/\omega_0)t$, hence in units of the external drive period, this period is $\omega_0/(\epsilon \times 0.77) = 12.98$ which is close to the period of the ensemble. The first peak in $\langle R^2 \rangle$ occurs at an amplitude of 2.63 which implies $\langle |u| \rangle_{max} \simeq \sqrt{\langle R^2 \rangle} = 1.62$. From fig. 10 we see that the zero energy particles have $u_{max} = 1.65$, again close to the ensemble average for the first maxima. As time progresses, the particles get increasingly out of phase with each other because of their differing frequencies so that the subsequent maxima in $\langle R^2 \rangle$ decrease in amplitude till eventually equilibrium is reached. A lower bound on the time to relax to equilibrium can be estimated in terms of the spread of frequencies $\Delta\Omega$ near the origin which is approximately 0.02 in this case. This leads to an estimate of $\omega_0/(\epsilon\Delta\Omega) \simeq 500$ periods of the external drive. Thus we expect equilibrium to set in after $500n$ where n is a reasonably small integer. The dashed line shows the statistical equilibrium calculation and the agreement is quite good. This is good numerical evidence in support of the discussion in Section 5.

Figure 21 shows the time evolution of the centroid $\langle u \rangle$ for the same values of the parameters and the behavior is similar. The fixed point is at $u = 1.02$ but the equilibrium value of the centroid is only 0.35 because, as can be seen in fig. 10, the phase curves have a larger fraction to the left of the fixed point.

In fig. 22 is shown the time evolution of the ensemble average of R^2 at a detuning above the bifurcation value. The amplitude equilibrates quickly compared to the case below the bifurcation value. To understand this we refer back to the frequency versus energy curves shown in figs. 13 and 14. Above the bifurcation value Δ_{bf}, the spread in frequencies in a given energy range is greater than it was below Δ_{bf}. The decoherence time and therefore the relaxation time is expected to be shorter for $\Delta > \Delta_{bf}$.

The equilibrium value of $\langle u^2 + v^2 \rangle$ as calculated with the equilibrium density agrees quite well with the long time limit obtained from the time evolution, as seen in figs. 22 and 23. For a more extensive comparison, we have calculated these two values for $\langle u^2 + v^2 \rangle$ at long times at values of Δ

in the range $-1.0 \leq \Delta \leq 2.0$ with the nonlinearity and forcing held constant at $\lambda = 3/8$ and $\kappa = 0.5$ respectively. These are shown in table 1.

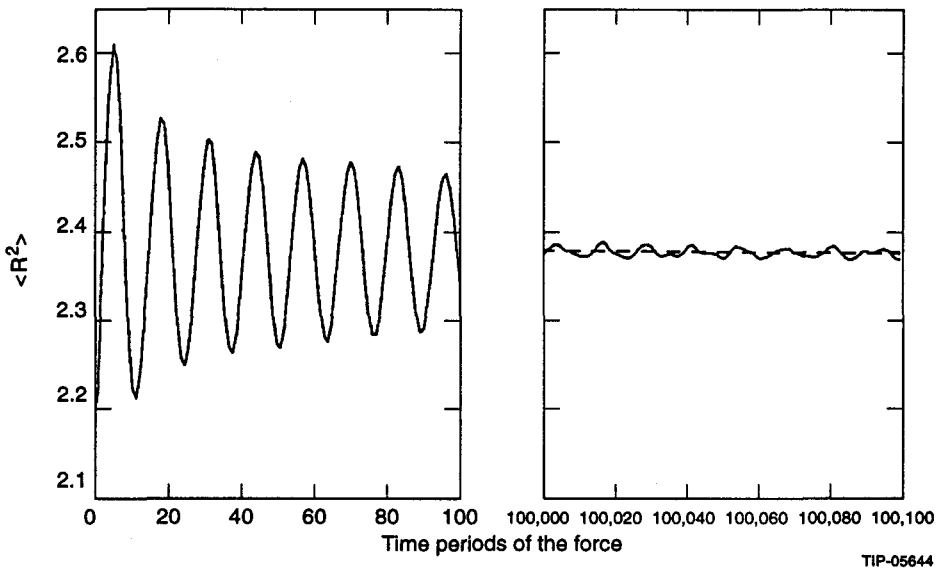

Fig. 20. Time evolution of $\langle R^2 \rangle$ calculated using the solutions found in Section 4.4 at a detuning below the bifurcation value: $\lambda = 3/8$, $\kappa = 0.5$, $\Delta = -0.1$. The line in dashes in the right half window represents the equilibrium value calculated from the equilibrium density distribution.

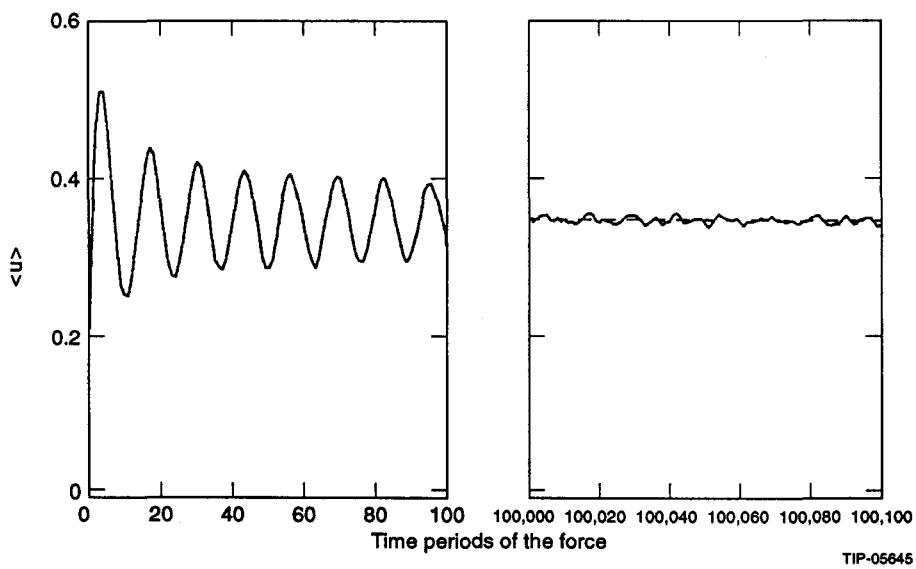

Fig. 21. Time evolution of $\langle u \rangle$ calculated using the solutions found in Section 4.4 at a detuning below the bifurcation value: $\lambda = 3/8$, $\kappa = 0.5$, $\Delta = -0.1$. The line in dashes in the right half window represents the equilibrium value calculated from the equilibrium density distribution.

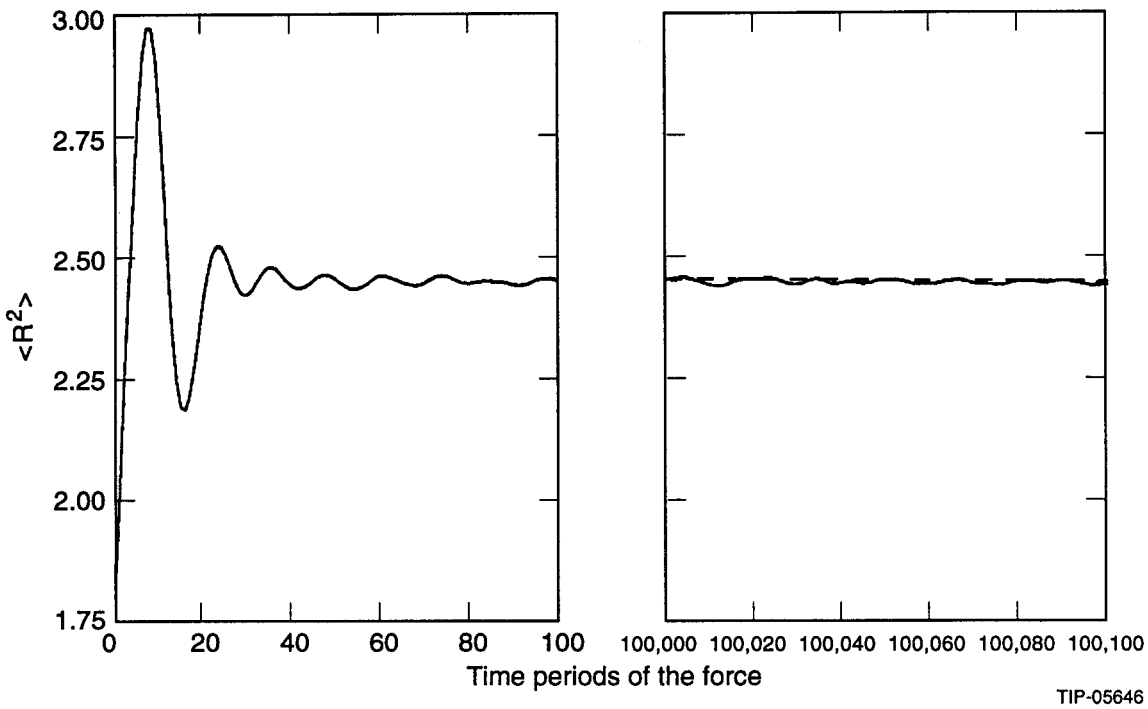

Fig. 22. Same as fig. 20 except at a detuning above the bifurcation value: $\lambda = 3/8$, $\kappa = 0.5$, $\Delta = 2.0$.

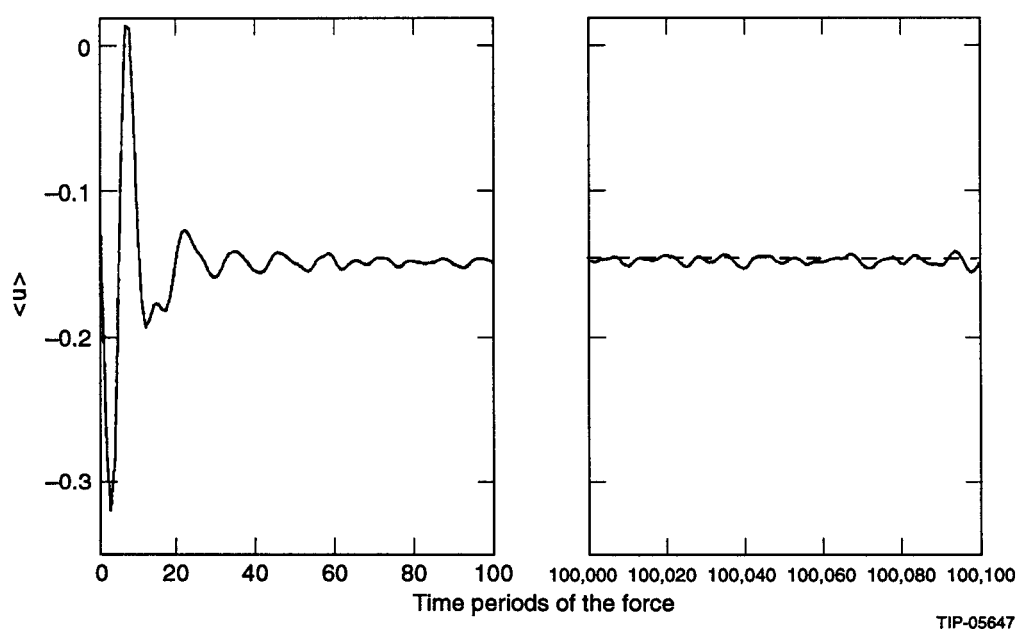

Fig. 23. Same as the fig. 21 except at a detuning above the bifurcation value: $\lambda = 3/8$, $\kappa = 0.5$, $\Delta = 2.0$.

Table 1. Comparison of the equilibrium ensemble average of $R^2 = u^2 + v^2$ calculated from the time evolution using the exact solutions with the statistical average using the equilibrium phase space density; $\lambda = 3/8, \kappa = 0.5$. For the limit from the time evolution, 10^5 particles were used with the average taken over 100 periods beginning at period 100,000.

Δ	Limit from time evolution	Statistical Average
−1.0	2.3388	2.3418
−0.75	2.3104	2.3127
−0.5	2.3067	2.3085
−0.25	2.3377	2.3390
−0.1	2.3779	2.3786
0.0	2.4145	2.4149
0.1	2.4598	2.4588
0.25	2.5423	2.5412
0.50	2.7146	2.7151
0.75	2.9150	2.9172
0.87	3.0040	3.0062
0.90	3.0165	3.0190
0.95	3.0284	3.0317
1.00	3.0324	3.0358
1.50	2.8226	2.8210
1.75	2.6357	2.6458
2.00	2.4486	2.4527

In most cases the agreement between the values of $\langle R^2 \rangle_{eq}$ obtained from the time evolution and that from the statistical evolution is of the order of 0.1%.

We must relate $\langle R^2 \rangle_{eq}$ to the quantity $\langle x^2 + \dot{x}^2/\omega_r^2 \rangle$ obtained by numerically integrating the original Duffing equations of motion. On a Poincaré surface of section,

$$\lim_{t \to \infty} \left\langle x^2 + \frac{\dot{x}^2}{\omega_r^2} \right\rangle \Bigg|_{t \text{ in Section}} = \langle R^2 \rangle_{eq} + O(\epsilon) \ . \tag{8.5}$$

Obviously the numerical integration is more computationally demanding than using exact solutions to follow the time evolution. We have limited the ensemble size to 10^4 particles and integrated the motion over the first 1000 periods of the force. Even this calculation in double precision, albeit without making any special effort to optimize the computer program, requires about 40 hours on a SUN Sparcstation 2. Table 2 shows the limit from the evolution calculated at a few values of Δ with other parameters held fixed.

Table 2. $\langle x^2 + \dot{x}^2/\omega_r^2 \rangle$ calculated with 10^4 particles and the following parameters: $\epsilon = 0.1, f = 1.0$. The time evolution is followed for 1000 periods with the average calculated over the last 500 periods. The evolution of $\langle u^2 + v^2 \rangle$ is calculated from the exact solutions with the same number of particles and over the same time period.

Δ	Limit from time evolution	
	$\langle x^2 + \dot{x}^2/\omega_r^2 \rangle$	$\langle u^2 + v^2 \rangle$
-1.0	2.483	2.363
-0.5	2.440	2.328
-0.1	2.512	2.397
0.25	2.689	2.558
0.75	3.106	2.930
0.87	3.197	3.018
1.0	3.206	3.047
1.5	2.923	2.847
2.0	2.482	2.486

The values of $\langle x^2 + \dot{x}^2/\omega_r^2 \rangle$ shown in this table should not be compared to the equilibrium values of $u^2 + v^2$ shown in table 1 because the number of particles used here is ten times smaller and the evolution is followed for a comparatively short time. Instead, to properly compare the two averages, we calculate $\langle u^2 + v^2 \rangle$ with the same number of particles and over the same time period using the exact solutions. These results, also seen in table 2, show that the maximum difference is about 0.18 which agrees with our expectation that the two values differ by $O(\epsilon)$ with $\epsilon = 0.1$. $\langle x^2 + \dot{x}^2/\omega_r^2 \rangle$ has a similar dependence on Δ as $u^2 + v^2$, peaking near $\Delta = 1.0$ for the chosen values of α and f.

9. Effect of detuning and forcing on amplitude growth

In this paper we are examining the collective behavior of an ensemble of non-interacting Duffing oscillators, each of which is governed by the equation

$$\ddot{x} + \omega_0^2 x + \epsilon \alpha x^3 = \epsilon f \cos \omega_r t \ . \tag{9.1}$$

We have seen that to first order in ϵ, the solution for x is

$$x = u \cos \omega_r t + v \sin \omega_r t + O(\epsilon) \tag{9.2}$$

on $O(1/\epsilon)$ time intervals. The variables (u, v) describe the slower oscillations of the envelope of x, their evolution is obtained from an autonomous Hamiltonian system (4.25) and (4.26). The prob-

lem of describing the collective behavior is thus reduced to describing the equilibrium statistical mechanics of a time independent Hamiltonian system.

We have seen that the average amplitude (or equivalently emittance) rises quickly to a maximum value and then relaxes towards an equilibrium value, undergoing smaller amplitude oscillations in the process. The equilibration occurs within a few periods of the external force if the detuning Δ (where $\omega_r = \omega_0 + \epsilon\Delta$) is greater than the value $\Delta_{bf} = 3(\lambda\kappa^2/4)^{1/3} = (3/4\omega_0)[3\alpha f^2/2]^{1/3}$ and takes considerably longer if $\Delta < \Delta_{bf}$. This can be understood in terms of the frequency spread of the autonomous system.

The equilibrium value of the average amplitude predicted by the use of the equilibrium phase space density $\rho_{eq}(u,v)$ in (u,v) space agrees to $O(\epsilon)$ with the average amplitude calculated for the $(x,\dot{x})$ system by numerical simulation of the time evolution of 10^4 particles in the cases we have considered. This justifies the use of the equilibrium values found using $\rho_{eq}(u,v)$ to answer questions about the collective behavior posed in Section 1 *viz.*, the effect of the detuning Δ and force amplitude f on the amplitude growth.

9.1. Effect of the detuning

When $\Delta < \Delta_{bf}$ there is only one fixed point in the (u,v) phase space and the amplitude growth increases as Δ increases. This is simply because the fixed point increases in amplitude as Δ increases, causing the particles at the center of the phase space where the initial detuning is largest to oscillate with larger and larger amplitudes as can be seen from figs. 8, 10 and 11. This will be seen in figs. 24–26.

For $\Delta > \Delta_{bf}$, there are three fixed points (two of which are stable), and the effect of the detuning depends on the magnitude of the force. We can define a length scale L_f associated with the force: this length being the distance of the unstable fixed point from the origin of phase space at the bifurcation value Δ_{bf} of the detuning. From Section IV.B we have

$$L_f = \sqrt{\frac{\Delta_{bf}}{3\lambda}} = \left[\frac{\kappa}{2\lambda}\right]^{1/3} = \left[\frac{2f}{3\alpha}\right]^{1/3} . \tag{9.3}$$

The effect of the detuning depends on the initial beam (or distribution) size relative to this length scale. Let $\langle R_0\rangle = \langle\sqrt{u_0^2+v_0^2}\rangle$ denote the initial average radius in (u,v) phase space. We can distinguish three regimes:

i) $L_f \ll \langle R_0\rangle$, i.e very weak forcing,
ii) $L_f \sim \langle R_0\rangle$, moderate forcing,
iii) $L_f > \langle R_0\rangle$, large forcing.

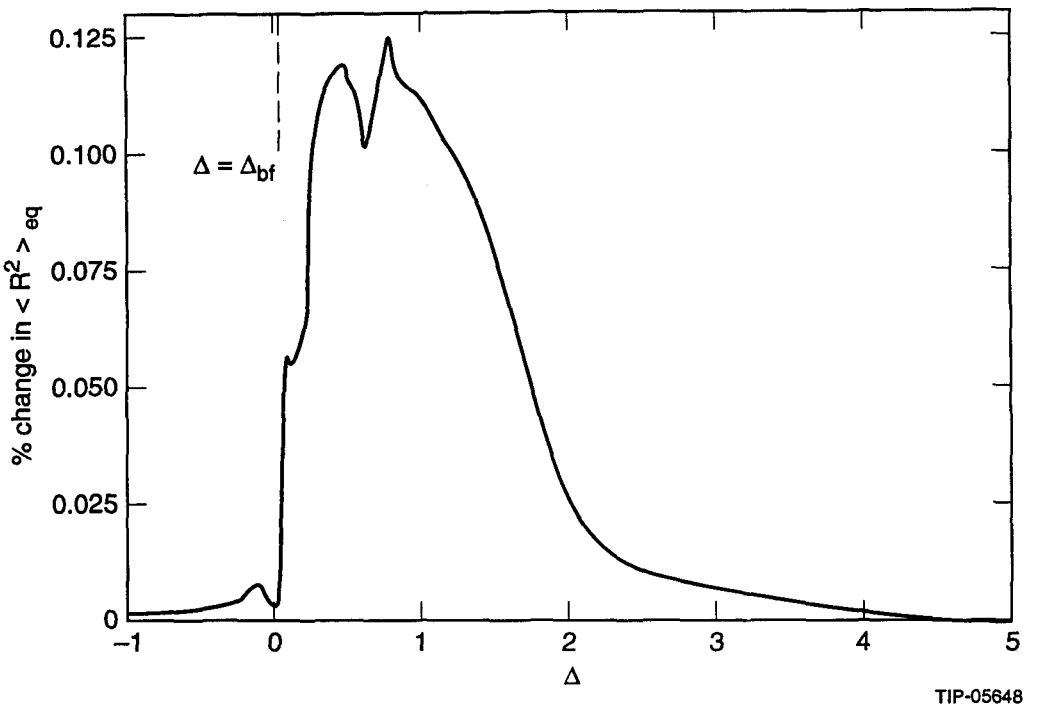

Fig. 24. Average amplitude squared as a function of the detuning for very small forcing; $\lambda = 3/8$, $\kappa = 0.005$, $\Delta_{bf} = 0.04$.

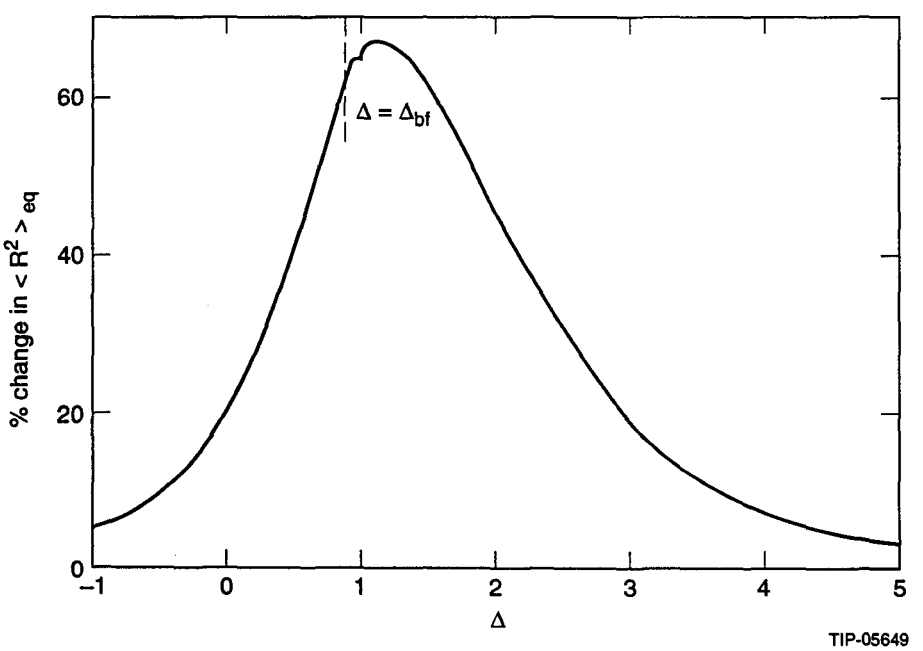

Fig. 25. Average amplitude squared as a function of the detuning for moderate forcing; $\lambda = 3/8$, $\kappa = 0.5$, $\Delta_{bf} = 0.859$.

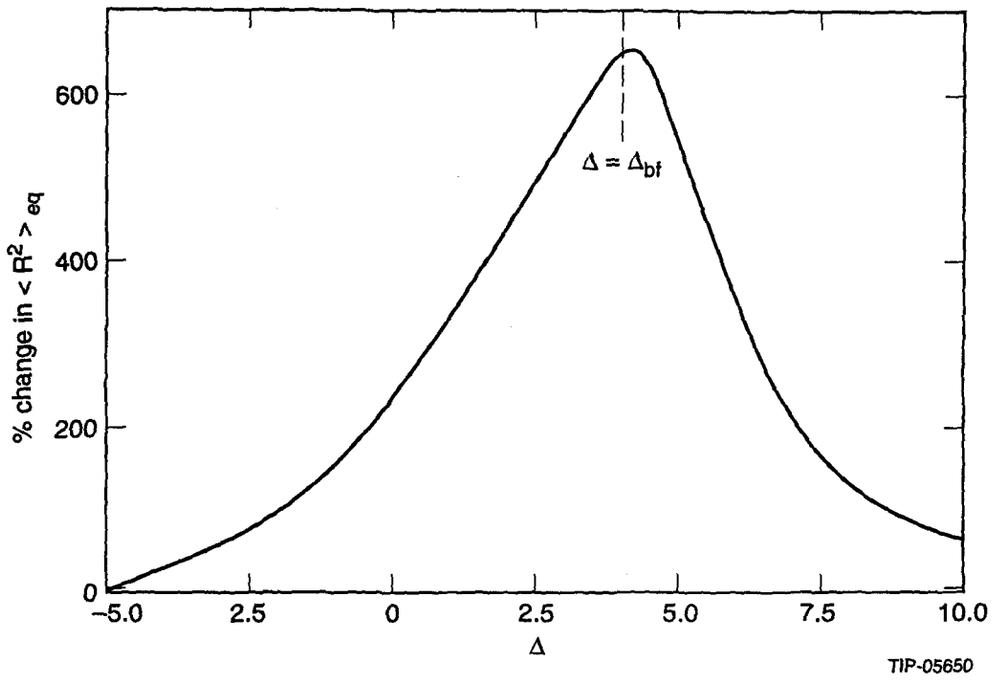

Fig. 26. Average amplitude squared as a function of the detuning for large forcing; $\lambda = 3/8$, $\kappa = 5.0$, $\Delta_{bf} = 3.985$.

We consider each of these regimes in turn. To follow the discussion the reader may wish to refer to fig. 8 for the dependence of fixed point amplitudes on the detuning and fig. 12 for the phase portrait. Although we have considered only Gaussian density distributions in our calculations, the following results will hold for any initial density distribution that is somewhat localized near the origin of phase space.

i) $L_f \ll \langle R_0 \rangle$. In this case the beam is much bigger than the amplitude a_3 at which the unstable fixed point first appears and also much bigger than a_1. As Δ increases beyond Δ_{bf} the stable fixed point a_1 moves outward from the origin while the stable fixed point a_2 moves in towards the origin. Initially the phase space contours going through the origin (the region of high initial density) encircle a_1 so that the amplitude growth will increase with Δ. However when the detuning reaches a value Δ_1 such that the fixed point a_1 is at the initial average radius, the equilibrium average amplitude will start to decrease since now most particles will be moving on small ovals around the other stable fixed point a_2. This value of Δ_1 is given by

$$a_1 = 2\sqrt{\frac{\Delta_1}{3\lambda}} \cos\left[\frac{1}{3}\cos^{-1}\left(\frac{\Delta_{bf}}{\Delta_1}\right)^{3/2}\right] \sim \langle R_0 \rangle \ . \tag{9.4}$$

Assuming that $\Delta_{bf} \ll \Delta_1$, we can approximate $\cos^{-1}[\Delta_{bf}/\Delta_1]^{3/2} \approx \pi/2 - [\Delta_{bf}/\Delta_1]^{3/2}$. Since $\Delta_{bf}^{3/2}$ is linear in κ, we expand the cosine factor to terms linear in κ. Δ_1 then obeys the equation $\Delta_1^{3/2} - \sqrt{\lambda}\langle R_0\rangle\Delta_1 + \kappa\sqrt{\lambda}/2 = 0$. Solving this to first order in κ, we obtain

$$\Delta_1 = \lambda\langle R_0\rangle^2 - \frac{\kappa}{\langle R_0\rangle} \quad . \tag{9.5}$$

The first term clearly dominates, so that at very small forcing, the detuning which causes the maximum amplitude growth is nearly a constant, equal to $\lambda\langle R_0\rangle^2$, which depends only on the initial beam size and the nonlinearity parameter. We also note that in the absence of forcing, the frequency of the non-linear oscillator at an amplitude $\langle R_0\rangle$ is $\omega_0 + \epsilon\lambda\langle R_0\rangle^2$ so we obtain the condition that the external drive frequency $\omega_r = \omega_0 + \epsilon\Delta_1$ must equal the frequency at approximately 1 sigma of the beam size for the maximum growth in amplitude.

For the numerical calculation of the equilibrium $\langle R^2\rangle$ at very small forcing, we use the exact solutions and calculate the ensemble average over 10^5 particles after 10^6 periods and the time average is over 500 periods. The errors in this calculation are smaller than the errors in the numerical integration using the equilibrium density. Figure 24 shows the percentage change in $\langle R^2\rangle_{eq}$ as a function of the detuning at $\kappa = 0.005$ and note that it is quite small. The effect on $\langle R^2\rangle_{eq}$ is also very small and we believe that the dip at $\Delta = 0.6$ is an artifact of the calculation. The maximum occurs in the vicinity of $\Delta = 0.75$. We can compare this to our estimate for Δ_1. $\langle R_0\rangle \approx \sqrt{\sigma_x^2 + \sigma_x^2} = \sqrt{2}$, so we obtain $\Delta_1 \approx 2\lambda - \kappa/\sqrt{2} = 0.746$ which is very close to the numerical data.

ii) $L_f \sim \langle R_0\rangle$. The initial size of the beam is now comparable to the distance to the unstable fixed point at Δ_{bf} where the stable fixed point a_1 is at distance $2L_f$. For $\Delta > \Delta_{bf}$ there is a competition for particles in the distribution between the fixed points a_1 and a_2. The average amplitude increases with Δ until a value Δ_2 is reached such that the inner homoclinic loop encircling a_2 passes through the origin. Beyond this value of Δ, particles initially close to the origin will move around a_2 and the average amplitude will decrease.

We can calculate the value Δ_2 of Δ at which the homoclinic loop goes through the origin. Setting the energy on the homoclinic loop to zero and using Eq. (4.17) for the fixed point amplitude, we obtain

$$\Delta_2 = 3\left(\frac{1}{2}\lambda\kappa^2\right)^{1/3} = 2^{1/3}\Delta_{bf} \ . \tag{9.6}$$

Thus for moderate forcing, the growth in amplitude has a maximum in the range of detuning Δ given by

$$\Delta_{bf} < \Delta < 2^{1/3}\Delta_{bf} \quad . \tag{9.7}$$

To consider a specific case, at $\lambda = 3/8, \kappa = 0.5$, the homoclinic loop goes through the origin at $\Delta_2 = 1.082$ while the maximum growth in R^2 occurs near $\Delta = 1.1$, as seen in fig. 25. The bifurcation

value is $\Delta_{bf} = 0.859$. Note that at this moderate value of the forcing, the equilibrium value changes quite dramatically depending on the driving frequency, ranging from 5% at $\omega_r = \omega_0 - 0.1$ to nearly 68% at $\omega_r = \omega_0 + 0.1$ and back down to 4% at $\omega_r = \omega_0 + 0.5$.

iii) $L_f > \langle R_0 \rangle$. The fixed points are beyond the initial average beam radius. We assume that the forcing is not too large so that first order perturbation theory is still applicable. Since the stable fixed point a_2 is initially just at the edge of the beam, it follows that with an increase in Δ beyond Δ_{bf} more particles will be trapped around a_2 than around a_1 which moves even further away. Hence for this case we expect that the average amplitude will increase till Δ_{bf} and decrease thereafter.

Figure 26 shows the growth in $\langle R^2 \rangle_{eq}$ over a range of Δ at the large forcing amplitude $\kappa = 5.0$. The peak in the growth occurs very near the bifurcation value $\Delta_{bf} = 3.985$ as expected.

We see from the results that as the forcing amplitude increases, the ratio Δ/Δ_{bf} at which the largest growth in amplitude occurs decreases, from a high value of $\lambda\langle R_0^2 \rangle/\Delta_{bf}$ at very weak forcing to a low value of 1 at large forcing.

9.2. Effect of the forcing amplitude

We have seen that the equilibrium value $\langle R^2 \rangle_{eq}$ attains its maximum at a particular detuning value in each of the three regimes of force amplitude f. If the detuning is held constant, $\langle R^2 \rangle_{eq}$ increases monotonically as f is increased. However the growth rates are different in the three regimes.

We examine first the case of very weak forcing. Figure 27 shows the relative change in $\langle R^2 \rangle_{eq}$ as κ varies from 0.001 to 0.01. The straight lines are least square fits to the data points marked by different symbols. Almost over the entire range the growth is larger at $\Delta = 0.75$ than at the other two values $\Delta = 0.5$ and $\Delta = 1.0$ on either side of it. This is consistent with fig. 24 and our analysis in the previous subsection. At the largest value of κ in this figure, the growth at $\Delta = 0.5$ is slightly larger. This is also to be expected since with increasing force the "resonant" value of Δ decreases towards Δ_{bf}.

Doing a least squares fit for the slopes of the lines shown in fig. 27 gives the following power law dependences,

$$\Delta = 0.50: \quad \frac{\Delta R^2}{R^2} = (2.81 \pm 0.01)\kappa^{(1.47 \pm 0.05)}$$

$$\Delta = 0.75: \quad \frac{\Delta R^2}{R^2} = (1.90 \pm 0.01)\kappa^{(1.38 \pm 0.04)}$$

$$\Delta = 1.00: \quad \frac{\Delta R^2}{R^2} = (2.33 \pm 0.01)\kappa^{(1.44 \pm 0.04)} \quad .$$

This shows that in the very weak forcing regime, the equilibrium value scales with the force roughly as $\kappa^{1.4}$.

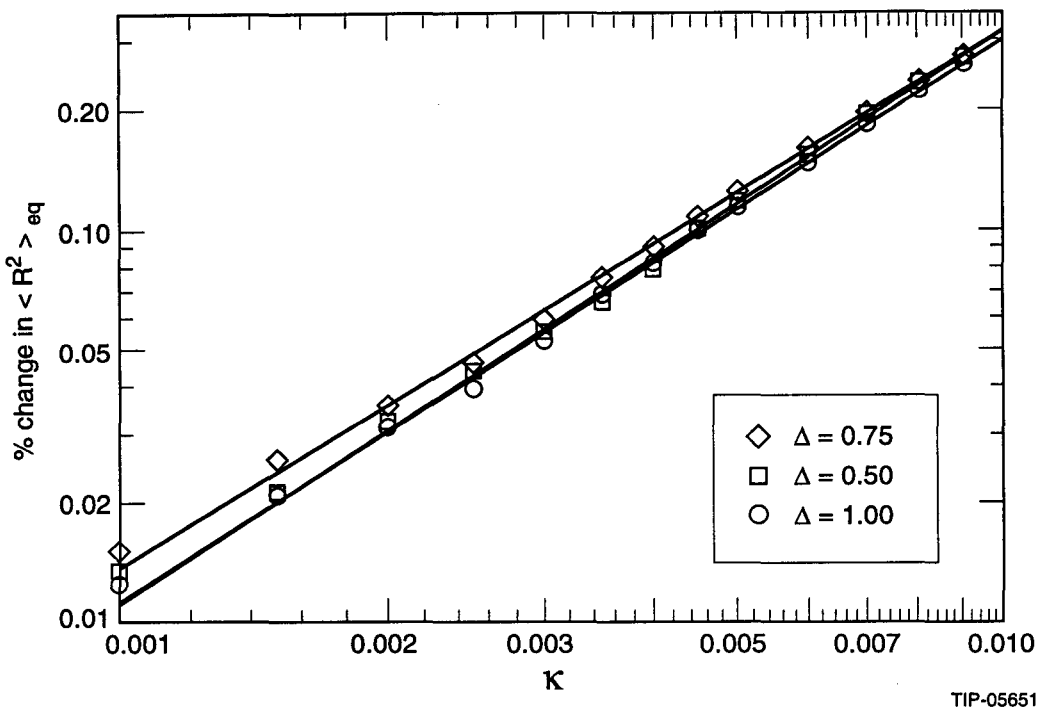

Fig. 27. Change in $\langle R^2 \rangle_{eq}$ as a function of the forcing amplitude at three values of the detuning just above the bifurcation value in the regime of very small to small forcing; $\epsilon = 0.1$. Both the abscissa and the ordinate are plotted on a log scale.

We can try to estimate the dominant source of this amplitude growth. Since $\Delta \gg \Delta_{bf}$ and κ is very small, the stable fixed point at $-a_2$ is very close to the origin, in fact $a_2 = \kappa/\Delta$ to first order in κ. The other stable fixed point is at $a_1 = \sqrt{\Delta/\kappa} + \kappa/(2\Delta)$ and the unstable fixed point is at $-a_3 = -\sqrt{\Delta/\kappa} + \kappa/(2\Delta)$. Particles close to the origin move in stable elliptic orbits around $-a_2$. We can estimate the contribution of these particles to the equilibrium value of $\langle R^2 \rangle_{eq}$ by calculating

$$\langle u^2 + v^2 \rangle_2 = \int\int (u^2 + v^2) \rho_{eq} \Big[H(u,v) \Big] \, du \, dv \quad ,$$

where the subscript 2 denotes the contribution from particles moving around $-a_2$. We expand ρ_{eq} and $H(u,v)$ in a Taylor series about the fixed point and use the expression in Eq. (6.6) for ρ'_{eq}. Subtracting the initial value of $\langle u^2 + v^2 \rangle$ for these particles, we find that the relative change $\delta\langle u^2 + v^2 \rangle / \langle u^2 + v^2 \rangle$ to be $O(\kappa^2)$. This can be understood qualitatively by the fact that the difference between the semi-major and semi-minor axes of these elliptic orbits is of $O(\kappa^2)$ and there would be no change in $\langle u^2 + v^2 \rangle$ if the orbits were circular. From the numerics we see that $\langle u^2 + v^2 \rangle$ grows faster than κ^2, i.e. with smaller exponent, at very small κ so we expect that the dominant contribution comes from particles moving in the kidney shaped orbits around the stable fixed point a_1.

In the regimes of moderate and strong forcing we expect from our previous analysis that the "resonant" value of Δ to be closer to the bifurcation value Δ_{bf}. Figures 28 and 29 show the relative change in $\langle R^2 \rangle_{eq}$ for moderate and strong forcing respectively at three values close to Δ_{bf}. In both these figures, the equilibrium values have been calculated using the equilibrium density distribution. Note that for moderate forces there is a crossover of the detuning $\Delta = 1.5\Delta_{bf}$ from having the strongest effect at the low end of the forcing scale to having the weakest effect at the higher end. In the range $0.4 \leq \kappa \leq 1.0$, the detuning $\Delta = \Delta_U = 2^{1/3}\Delta_{bf}$ has the strongest effect as predicted by our analysis. For strong forcing the largest effect occurs at the bifurcation value Δ_{bf}. Over the range of κ shown in fig. 29, the equilibrium value grows roughly as $\kappa^{0.9}$ at $\Delta = \Delta_{bf}$, a slightly slower than linear growth. This result cannot be extrapolated to larger force amplitudes since then first order perturbation theory will be inadequate.

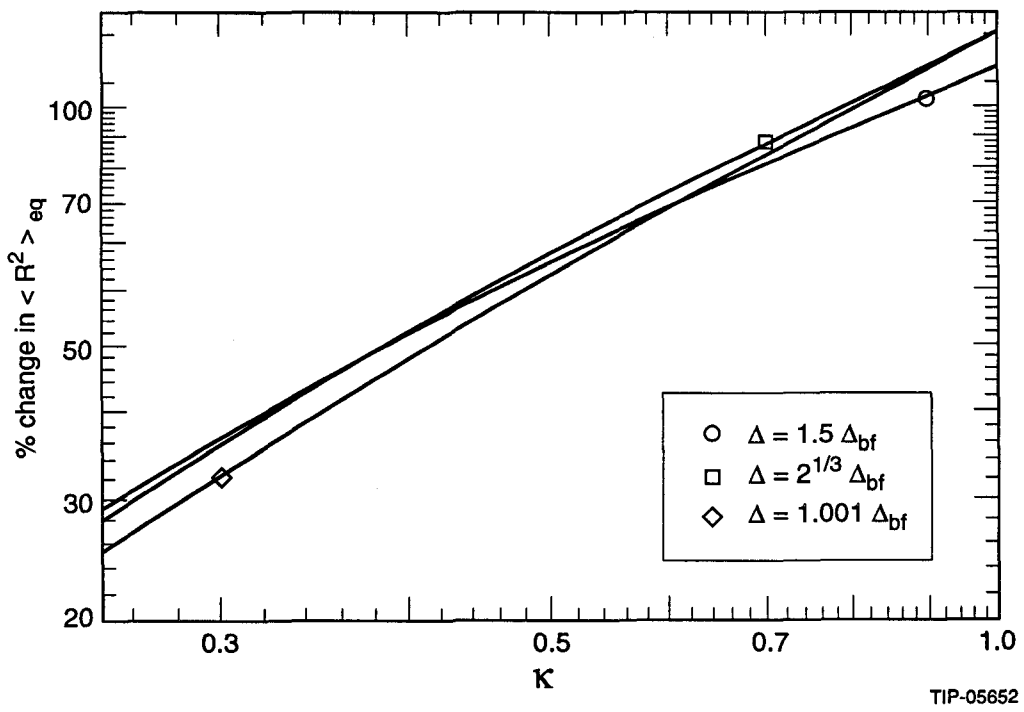

Fig. 28. Same as fig. 27 but in the regime of moderate forcing; $\epsilon = 0.1$.

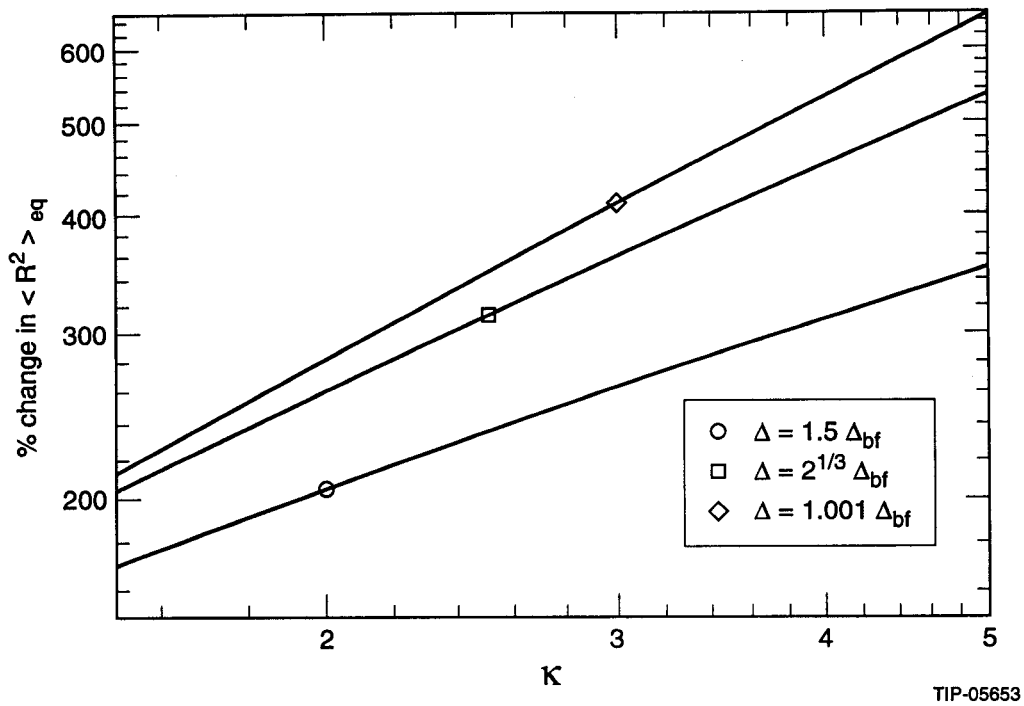

Fig. 29. Same as fig. 28 but in the regime of large forcing; $\epsilon = 0.1$.

10. Summary

In this paper we have studied the long time behavior of an ensemble of particles evolving according to the forced Duffing equation with small nonlinearity parameter ϵ. An initial density $\rho_0(\mathbf{x})$ evolves incompressibly to $\rho(\mathbf{x}, t)$ at time t, as discussed in Appendix B, and we have investigated the long time behavior of phase space averages defined by

$$\Big\langle f(\mathbf{x}) \Big\rangle(t) = \int_{\text{all phase space}} f(\mathbf{x})\rho(\mathbf{x}, t)\ d\mathbf{x} \ .$$

The numerical evidence of Section 3 indicates that the centroid and the average amplitude squared of the ensemble settle down to an equilibrium value at long times. From our analysis we conjecture that the phase space averages should have a long time limit based on two facts: 1) the solution of the Duffing equation can be approximated by an autonomous system on time intervals of $O(1/\epsilon)$ and possibly $O(1/\epsilon^2)$ as discussed in Section 4.1 and 2) the ensemble density for the autonomous system has a long time coarse grained limit due to the phase mixing amongst particles of different frequencies as discussed in Section 5. This equilibrium density, ρ_{eq}, is a function only of the energy of the autonomous system and is given by the time average of the initial density over the curve of that energy.

Both the equilibrium density and the phase space averages depend crucially on the detuning parameter Δ. Above the bifurcation value Δ_{bf}, where there are three fixed points in the phase portraits of the autonomous system, there is a two-fold degeneracy of curves with the same energy and ρ_{eq} has a jump discontinuity. Below Δ_{bf}, ρ_{eq} is a smooth function of the energy. Phase space averages of the autonomous system using the equilibrium density can be compared with the limit obtained by numerically ensemble averaging the exact solutions (obtained in Section 4.4) of this system. We find in Section 8 that the agreement between the values calculated the two ways agree to within 0.1%. This lends additional support to the conjecture that phase space averages equilibrate at long times.

The effect of the forcing amplitude and detuning on the amplitude growth can best be understood by comparing the initial average size $\langle R_0 \rangle$ of the ensemble (i.e. the average radius of the beam) to the distance L_f of the unstable fixed point from the origin at the bifurcation value Δ_{bf} of the detuning. For very weak forcing ($L_f \ll \langle R_0 \rangle$), the regime of interest in the application to emittance growth due to power supply ripple, the maximum growth occurs when the external frequency is in a neighborhood of the frequency of the unforced nonlinearly oscillating particles at distance $\langle R_0 \rangle$ from the origin. For moderate and strong forcing, the maximum growth occurs when the detuning is in the neighborhood of the bifurcation value Δ_{bf}. We also find in the weak forcing regime that the amplitude growth scales roughly as the 7/5 power of the force. This can be used to estimate the level to which the ripple field must be reduced to avoid substantial emittance growth.

In this paper we considered only the nonlinearity resulting from the magnetic fields. The dominant nonlinearity in many accelerators however comes from the beam-beam interaction which results in a very different nonlinear potential. Wake fields generated by a beam within a vacuum chamber also react back on the beam leading to other instabilities. We hope to consider the effects of power supply ripple in the presence of these phenomena in a subsequent publication.

Acknowledgements

We thank Richard Talman and Mike Syphers for useful discussions and encouragement.

Appendix A: First Order Averaging Theory

Here we sketch the first order averaging theory necessary for the paper. The initial value problem (IVP) we want to approximate is

$$\frac{d}{d\tau}\mathbf{y} = \epsilon\mathbf{G}(\mathbf{y},\tau) + \epsilon^2\mathbf{R}_1(\mathbf{y},\tau,\epsilon)$$

$$\mathbf{y}(\tau_0) = \mathbf{x}_0 \ , \tag{A.1}$$

where $\mathbf{G}$ is $2\pi-$ periodic in τ. We define the averaged IVP

$$\frac{d}{d\tau}\mathbf{u} = \epsilon\bar{\mathbf{G}}(\mathbf{u})$$

$$\mathbf{u}(\tau_0) = \mathbf{x}_0 \ , \tag{A.2}$$

and the guiding IVP

$$\frac{d}{d\tau}\mathbf{v} = \bar{\mathbf{G}}(\mathbf{v})$$

$$\mathbf{v}(0) = \mathbf{x}_0 \ , \tag{A.3}$$

where

$$\mathbf{G}(\mathbf{y},\tau) = \bar{\mathbf{G}}(\mathbf{y}) + \tilde{\mathbf{G}}(\mathbf{y},\tau) \tag{A.4}$$

and $\bar{\mathbf{G}}$ is the average of $\mathbf{G}$ and $\tilde{\mathbf{G}}$ is the zero average part of $\mathbf{G}$. The solution of (A.2) can be written in terms of (A.3) as $\mathbf{u}(\tau) = \mathbf{v}(\epsilon(\tau-\tau_0))$. Let $\mathbf{G}$ and $\mathbf{R}_1$ be defined on $U\times\mathcal{R}$ where U is open in $\mathcal{R}^n$. Let $S = \{\mathbf{v}(s)|0 \le s \le T\}$ where T is appropriately chosen such that $\mathbf{v}(s)$ exists on $[0,T]$. Let U_1 be an open, bounded subset of U such that $S \subset U_1 \subset U$. Assume that $\mathbf{G}$ is y-Lipschitz on $\bar{U}_1$, the closure of U_1, with Lipschitz constant L, i.e. $|\mathbf{G}(\mathbf{y}_1,\tau) - \mathbf{G}(\mathbf{y}_2,\tau)| \le L|y_1 - y_2|$ for y_1, y_2 in U_1, and that R is bounded on $\bar{U}_1$ with bound M_1. It follows that as long as $\mathbf{y}(\tau)$ stays in U_1,

$$|\mathbf{y}(\tau) - \mathbf{u}(\tau)| = \left|\epsilon\int_{\tau_0}^{\tau}\Big[\mathbf{G}\Big(\mathbf{y}(s),s\Big) - \mathbf{G}\Big(\mathbf{u}(s),s\Big)\Big]\ ds + \epsilon\int_{\tau_0}^{\tau}\tilde{\mathbf{G}}\Big(\mathbf{u}(s),s\Big)\ ds + \epsilon^2\int_{\tau_0}^{\tau}\mathbf{R}\Big(\mathbf{y}(s),s,\epsilon\Big)\ ds\right|$$

$$\le \epsilon L\int_{\tau_0}^{\tau}\Big|\mathbf{y}(s) - \mathbf{u}(s)\Big|\ ds + \epsilon^2 M_1(\tau-\tau_0) + \epsilon\left|\int_{\tau_0}^{\tau}\tilde{\mathbf{G}}\Big(\mathbf{u}(s),s\Big)\ ds\right| \ , \tag{A.5}$$

where the equality is obtained by subtracting (A.2) from (A.1) and integrating from τ to τ_0. Now for fixed u, $\tilde{\mathbf{G}}(\mathbf{u},s)$ has zero average and $\mathbf{u}(s)$ is slowly varying so one might expect that the third term on the right hand side of (A.5) would remain $O(\epsilon)$ on time intervals $0 \le \epsilon(\tau-\tau_0) \le T$. In fact, by a generalization of a result of Besjes (see [17], Lemma 5), there exists a constant M_2 such that $|\int_{\tau_0}^{\tau}\tilde{\mathbf{G}}(\mathbf{u}(s),s)| \le M_2(\epsilon(\tau-\tau_0)+1)$ and we obtain

$$\left|\mathbf{y}(\tau)-\mathbf{u}(\tau)\right| \leq \epsilon M(T)+\epsilon L \int_{\tau_0}^{\tau}\left|\mathbf{y}(s)-\mathbf{u}(s)\right| \, ds \tag{A.6}$$

for $0 \leq \epsilon(\tau-\tau_0) \leq T$ and $\mathbf{y}(\tau)$ in U_1. It follows from the Gronwall inequality that

$$\left|\mathbf{y}(\tau)-\mathbf{u}(\tau)\right| \leq \epsilon M(T) \exp\left[\epsilon L(\tau-\tau_0)\right] \leq \epsilon C(T) \tag{A.7}$$

under the same conditions. At this point there is no restriction on ϵ, but we have assumed that τ is such that $\mathbf{y}(\tau)$ is in U_1. However, it can be shown that for ϵ small enough, $\mathbf{y}(\tau)$ exists in U_1 on time intervals $[0, T/\epsilon]$ and (A.7) gives the standard first order averaging result, viz.,

$$\mathbf{y}(\tau)=\mathbf{u}(\tau)+O(\epsilon) \tag{A.8}$$

for $0 \leq \epsilon(\tau-\tau_0) \leq T$.

With a little more work, using a transformation approach [17], it can be shown that

$$\mathbf{y}(\tau)=\mathbf{u}(\tau)+\epsilon \mathbf{P}\left(\mathbf{u}(\tau), \tau\right)+O\left(\epsilon^2(\tau-\tau_0)\right) \quad , \tag{A.9}$$

where

$$\mathbf{P}(\mathbf{u}, \tau)=\int_{\tau_0}^{\tau} \tilde{\mathbf{G}}(\mathbf{u}, s) \, ds \tag{A.10}$$

which improves the approximation at $O(1)$ times.

Appendix B: Solution of Liouville's Equation

Consider an ensemble of particles, each of which moves in the same force field. Let $\mathbf{x}$ denote the phase space variables for an individual particle and let its equation of motion be

$$\frac{d}{dt}\mathbf{x}=\mathbf{f}(\mathbf{x}, t)$$

$$\mathbf{x}(t_0)=\mathbf{x}_0 \quad , \tag{B.1}$$

with the general solution

$$\mathbf{x}(t)=\vec{\phi}(t, t_0, \mathbf{x}_0) \quad . \tag{B.2}$$

Let $\rho_0(\mathbf{x})$ be the initial phase space density and $\rho(\mathbf{x}, t)$ the time dependent density. At time t_0 we pick a region $\mathcal{A}$ in phase space containing some fraction of the particles and follow the evolution of this region in time. Let $\mathcal{A}_t$ denote this region at time t. Since no particles enter or leave this region, it follows that

$$\int_{\mathcal{A}} \rho_0(\mathbf{x}_0) \, d\mathbf{x}_0=\int_{\mathcal{A}_t} \rho(\mathbf{x}, t) \, d\mathbf{x} \quad . \tag{B.3}$$

Making the change of variable $\mathbf{x} \rightarrow \mathbf{x}_0$ via $\mathbf{x}(t) = \vec{\phi}(t, t_0, \mathbf{x}_0)$ transforms the integral on the right hand side of the above equation to $\int_{\mathcal{A}} \rho(\vec{\phi}(t, t_0, \mathbf{x}_0), t) J(t, \mathbf{x}_0)\, d\mathbf{x}_0$ where $J(t, \mathbf{x}_0)$ is the Jacobian of the transformation. We assume the functions involved are continuous. Since $\mathcal{A}$ is arbitrary

$$\rho_0(\mathbf{x}_0) = \rho\Big(\vec{\phi}(t, t_0, \mathbf{x}_0), t\Big) J(t, \mathbf{x}_0) \ . \tag{B.4}$$

Now $J(t, \mathbf{x}_0) = \det \partial\vec{\phi}(t, t_0, \mathbf{x}_0)/\partial\mathbf{x}_0$ is just the Wronskian associated with the variational equation for equation (B.1) and thus

$$J(t, \mathbf{x}_0) = \exp\left[\int_{t_0}^{t} \mathrm{Trace} \frac{\partial \mathbf{f}\Big(\vec{\phi}(s, t_0, \mathbf{x}_0), s\Big)}{\partial\vec{\phi}}\, ds\right] \tag{B.5}$$

and we obtain

$$\rho(\mathbf{x}, t) = \rho_0\Big(\vec{\phi}(t_0, t, \mathbf{x})\Big) \exp\left[-\int_{t_0}^{t} \mathrm{Trace} \frac{\partial \mathbf{f}\Big(\vec{\phi}(s, t, \mathbf{x}), s\Big)}{\partial\vec{\phi}}\, ds\right] \ , \tag{B.6}$$

where we have replaced $\mathbf{x}_0$ by $\vec{\phi}(t_0, t, \mathbf{x})$. When the vector field is divergence-less, the trace of $\partial\mathbf{f}/\partial\vec{\phi}$ is zero and we obtain the result cited in the text, namely

$$\rho(\mathbf{x}, t) = \rho_0\Big(\vec{\phi}(t_0, t, \mathbf{x})\Big) \ . \tag{B.7}$$

From Eq. (B.3) it follows that

$$\frac{d}{dt}\left[\rho\Big(\vec{\phi}(t, t_0, \mathbf{x}_0), t\Big) J(t, \mathbf{x}_0)\right] = 0 \tag{B.8}$$

which shows that the density $\rho(\mathbf{x}, t)$ evolves via the Liouville equation [18]

$$\frac{\partial\rho}{\partial t} + \nabla \cdot \Big(\rho\mathbf{f}(\mathbf{x}, t)\Big) = 0 \ . \tag{B.9}$$

Appendix C: $\rho'_{eq}(E)$ at a stable fixed point

From Eq. (6.4) we obtain

$$\Big[\rho_{eq}(E)T(E)\Big]' = \rho_0\Big(\mathbf{x}_0(E)\Big)T'(E) + \int_0^{T(E)} \rho'_0\Big(\vec{\phi}\Big(\eta, \mathbf{x}_0(E)\Big)\Big)\vec{\phi}_E\Big(\eta, \mathbf{x}_0(E)\Big)\, d\eta \ , \tag{C.1}$$

where we have used $\vec{\phi}(T(E), \mathbf{x}_0(E)) = \vec{\phi}(0, , \mathbf{x}_0(E)) = \mathbf{x}_0(E)$ and the subscript E denotes the differentiation with respect to E. Taking the limit as $E \rightarrow E_c$ we obtain

$$\rho'_{eq}(E_c)T_c = \lim_{E \rightarrow E_c} \int_0^{T(E)} \rho'_0\Big(\vec{\phi}\Big(\eta, \mathbf{x}_0(E)\Big)\Big)\vec{\phi}_E\Big(\eta, \mathbf{x}_0(E)\Big)\, d\eta \ , \tag{C.2}$$

where $T_c = T(E_c)$. In an abuse of notation we let $\vec{\phi}(\eta, u_m(E)) = \vec{\phi}(\eta, \mathbf{x}_0(E))$ where $\mathbf{x}_0(E) = (u_m(E), 0)^T$ and $u_m(E) = u_{max}(E)$ as defined in Section 4 and make use of the following

$$\vec{\phi}\Big(\eta, u_m(E)\Big) = \mathbf{u}_c + D_2\vec{\phi}(\eta, u_c)\Big(u_m(E) - u_c\Big) + O\Big(\Big(u_m(E) - u_c\Big)^2\Big) \ , \tag{C.3}$$

$$\rho_0'\Big(\vec{\phi}\Big(\eta, u_m(E)\Big)\Big) = \rho_0'(\mathbf{u_c}) + \rho_0''(\mathbf{u_c})\Big[\vec{\phi}\Big(\eta, u_m(E)\Big) - \mathbf{u}_c\Big] + O\Big(\Big(u_m(E)\Big) - u_c\Big)^2 \ , \tag{C.4}$$

$$\vec{\phi}_E\Big(\eta, u_m(E)\Big) = D_2\vec{\phi}\Big(\eta, u_m(E)\Big)u_m'(E) \ , \tag{C.5}$$

$$D_2\vec{\phi}\Big(\eta, u_m(E)\Big) = D_2\vec{\phi}(\eta, u_c) + D_2^2\vec{\phi}(\eta, u_c)\Big[u_m(E) - u_c\Big]^2 + O\Big(u_m(E) - u_c\Big)^2 \tag{C.6}$$

where $\mathbf{u}_c = (u_c, 0)^T$ and D_2 denotes the derivative with respect to the second argument, then the integrand of the right hand side of (C.2) becomes

$$\rho_0'(\mathbf{u}_c)\mathbf{x}(\eta)u_m'(E) + \Big[\rho'(\mathbf{u}_c)D_2^2\vec{\phi}(\eta, u_c) + \rho''(\mathbf{u}_c)\Big(\mathbf{x}(\eta), \mathbf{x}(\eta)\Big)\Big]\Big(u_m(E) - u_c\Big)u_m'(E)$$

$$+O\Big(\Big(u_m(E) - u_c\Big)^2 u_m'(E)\Big) \equiv I + II + III \ . \tag{C.7}$$

Here ρ'' is the second derivative as a bilinear map and

$$\mathbf{x}(\eta) = \begin{pmatrix} \cos\sqrt{ab}\eta \\ -\sqrt{a/b}\sin\sqrt{ab}\eta \end{pmatrix} \tag{C.8}$$

where

$$a = -\left.\frac{\partial^2 H}{\partial u^2}\right|_{u_c,0} = 3\lambda u_c^2 - \Delta$$

$$b = -\left.\frac{\partial^2 H}{\partial u^2}\right|_{u_c,0} = \lambda u_c^2 - \Delta \ . \tag{C.9}$$

It can be shown that I gives no contribution to the limit because $\mathbf{x}(\eta)$ is periodic, with period $T_c = T(E_c)$, and zero mean. Also it can be shown that

$$\lim_{E\to E_c}\Big[u_m(E) - u_c\Big]u_m'(E) = -\frac{1}{a}$$

$$\lim_{E\to E_c}\Big[u_m(E) - u_c\Big]^2 u_m'(E) = 0 \ , \tag{C.10}$$

thus III gives no contribution in the limit and the contribution from II is

$$-\frac{1}{a}\int_0^{T_c}\Big[\rho'(\mathbf{u}_c)D_2^2\vec{\phi}(\eta, u_c) + \rho''(\mathbf{u}_c)\Big(\mathbf{x}(\eta), \mathbf{x}(\eta)\Big)\Big]\, d\eta \ . \tag{C.11}$$

The second term is easy to evaluate, for the first term we let $\vec{\psi}(\eta) = D_2^2\vec{\phi}(\eta, u_c)$, then ψ satisfies the IVP

$$\vec{\psi}' = \mathbf{f}'(\mathbf{u}_c)\vec{\psi} + \mathbf{f}''(\mathbf{u}_c)\Big(\mathbf{x}(\eta), \mathbf{x}(\eta)\Big) \tag{C.12}$$

$$\vec{\psi}(0) = \mathbf{0} \ ,$$

where $\mathbf{f}(\mathbf{u}) = (-\partial H/\partial v, \partial H/\partial u)^T$ is the vector field governing the flow. After a lengthy calculation using the solution of (C.12) we obtain

$$\rho'_{eq}(E_c) = \frac{\lambda u_c}{a^2 b}(a+3b)\frac{\partial \rho_0(u_c,0)}{\partial u} - \frac{1}{2}\left[\frac{1}{a}\frac{\partial^2 \rho_0(u_c,0)}{\partial u^2} + \frac{1}{b}\frac{\partial^2 \rho_0(u_c,0)}{\partial v^2}\right] \ . \tag{C.13}$$

References

[1] R.R. Ruth in *Physics of Particle Accelerators*, ed. M. Month & M. Dienes, AIP Conf. Proc. No. 153 (AIP, New York, 1987) .

[2] R.L. Warnock and R.R. Ruth, *Phys. Rev. Lett.*, **66**, (1991) 990.

[3] R.L. Warnock and R.R. Ruth, *Physica D*, **56**, (1992) 188.

[4] A. Chao et. al., *Phys. Rev. Lett.*, **61**, (1988) 2752.

[5] S.Y. Lee et. al., *Phys. Rev. Lett.*, **67**, (1991) 3768.

[6] M. Syphers et. al., *Phys. Rev. Lett.*, **71**, (1993) 719.

[7] J. Guckenheimer and P. Holmes,*Nonlinear Oscillations, Dynamical Systems, and Bifurcations of Vector Fields*, Springer Verlag, New York, 1983 .

[8] H.G. Hereward, "Landau Damping by Nonlinearity", CERN/MPS/DL 69-11.

[9] E.D. Courant and H.S. Snyder, *Annals of Physics*, **3**, (1958) 1.

[10] A. W. Chao,*Physis of Collective Instabilities in High Energy Accelerators*, John Wiley, New York, 1993,

[11] M.J. Lighthill,*Fourier Analysis and Generalised Functions*, Cambridge University Press, 1962 .

[12] L.F. Shampine and H.A. Watts, see G.E. Forsythe, M.A. Malcolm and C.B. Moler, *Computer Methods for Mathematical Applications*, Prentice Hall, 1977 .

[13] R.Cogburn and J.A. Ellison, *Comm. Math. Phys.*, **149**, (1992) 97.

[14] W.H. Press, S.A. Teukolsky, W.T. Vetterling and B.P. Flannery, *Numerical Recipes in Fortran*, 2nd Edition, Cambridge, 1992.

[15] P.F. Byrd and M.D. Friedman, *Handbook of Elliptic Integrals for Engineers and Scientists*, Springer Verlag, New York, 1971.

[16] J.A. Ellison and T. Guinn, *Phys. Rev. B*, **13**, (1976) 1880.

[17] J.A. Ellison, A.W. Sáenz and H.S. Dumas, *J. of Diff. Eq.*, **84**, (1990) 383 .

[18] C.W. Gardiner, *Handbook of Stochastic Methods*, 2nd Edition, Springer Verlag, New York, 1985.